Journal of Medicinal Chemistry

pubs.acs.org/jmc

Article

Structure-Guided Discovery of *cis*-Hexahydro-pyrido-oxazinones as Reversible, Drug-like Monoacylglycerol Lipase Inhibitors

Bernd Kuhn,* Martin Ritter, Benoit Hornsperger, Charles Bell, Buelent Kocer, Didier Rombach, Marius D. R. Lutz, Luca Gobbi, Martin Kuratli, Christian Bartelmus, Markus Bürkler, Raffael Koller, Paolo Tosatti, Iris Ruf, Melanie Guerard, Anto Pavlovic, Juliane Stephanus, Fionn O'Hara, Dennis Wetzl, Wiebke Saal, Martine Stihle, Doris Roth, Melanie Hug, Sylwia Huber, Dominik Heer, Carsten Kroll, Andreas Topp, Manfred Schneider, Jürg Gertsch, Sandra Glasmacher, Mario van der Stelt, Andrea Martella, Matthias Beat Wittwer, Ludovic Collin, Jörg Benz, Hans Richter, and Uwe Grether*

Cite This: *J. Med. Chem.* 2024, 67, 18448−18464

Read Online

ACCESS | Metrics & More | Article Recommendations | Supporting Information

ABSTRACT: Monoacylglycerol lipase (MAGL) is a key enzyme involved in the metabolism of the endogenous signaling ligand 2-arachidonoylglycerol, a neuroprotective endocannabinoid intimately linked to central nervous system (CNS) disorders associated with neuroinflammation. In the quest for novel MAGL inhibitors, a focused screening approach on a Roche library subset provided a reversible benzoxazinone hit exhibiting high ligand efficiency. The subsequent design of the three-dimensional *cis*-hexahydro-pyrido-oxazinone (*cis*-HHPO) moiety as benzoxazinone replacement enabled the combination of high MAGL potency with favorable ADME properties. Through enzymatic resolution an efficient synthetic route of the privileged *cis*-(4*R*,8*S*) HHPO headgroup was established, providing access to the highly potent and selective MAGL inhibitor **7o**. Candidate molecule **7o** matches the target compound profile of CNS drugs as it achieves high CSF exposures after systemic administration in rodents. It engages with the target in the brain and modulates neuroinflammatory processes, thus holding great promise for the treatment of CNS disorders.

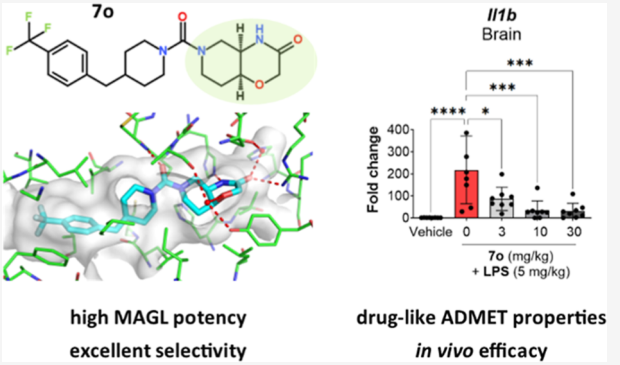

INTRODUCTION

Serine hydrolase monoacylglycerol lipase (MAGL)[1] is an essential regulator of the endocannabinoid system (ECS). The ECS encompasses a vast network of receptors and transporter proteins, endogenous signaling ligands, so-called endocannabinoids (eCBs), and enzymes that are responsible for eCB synthesis and degradation.[2] The ECS is an important lipid signaling system that is highly conserved among vertebrates and plays a key role in many human health and disease states. Most important eCBs are 2-arachidonylglycerol (2-AG) and *N*-arachidonoylethanolamine (AEA), locally produced and degraded by a majority of brain cells.[3] They bind to and activate type-1 and type-2 cannabinoid receptors (CB_1R and CB_2R, respectively), which are highly important targets for treating multiple human diseases ranging from metabolic to neurodegenerative disorders.[4] While both AEA and 2-AG behave as agonists for CB_1R, only 2-AG acts as a full agonist for CB_2R.[5−10] AEA and 2-AG are the predominant eCBs in the central nervous system (CNS). Brain 2-AG levels are significantly higher than AEA levels, e.g., ∼170 fold higher in murine brain.[11] MAGL is the key enzyme that controls the hydrolysis of 2-AG, and hence its biological activity. In the mouse brain, MAGL activity is responsible for degrading approximately 85% of 2-AG,[12] while the remainder is hydrolyzed by α,β-hydrolase domain containing protein 12 (ABHD12) and ABHD6. MAGL is a cytosolic membrane-bound serine hydrolase with two known isoforms of ∼33 and ∼35 kDa in mice and humans. 2-AG hydrolysis leads to the formation of glycerol and arachidonic acid (AA). 2-AG is the main source of AA production in the brain, which is then available for conversion to pro-inflammatory eicosanoids, including prostaglandins by cyclooxygenases COX1 and COX2.[13,14] This is in contrast to most peripheral tissues, where phospholipase A2 (PLA2), hydrolyzing membrane-bound phospholipids, is the major enzyme responsible for AA

Received: July 29, 2024
Revised: September 12, 2024
Accepted: September 17, 2024
Published: October 3, 2024

https://doi.org/10.1021/acs.jmedchem.4c01769
J. Med. Chem. 2024, 67, 18448−18464

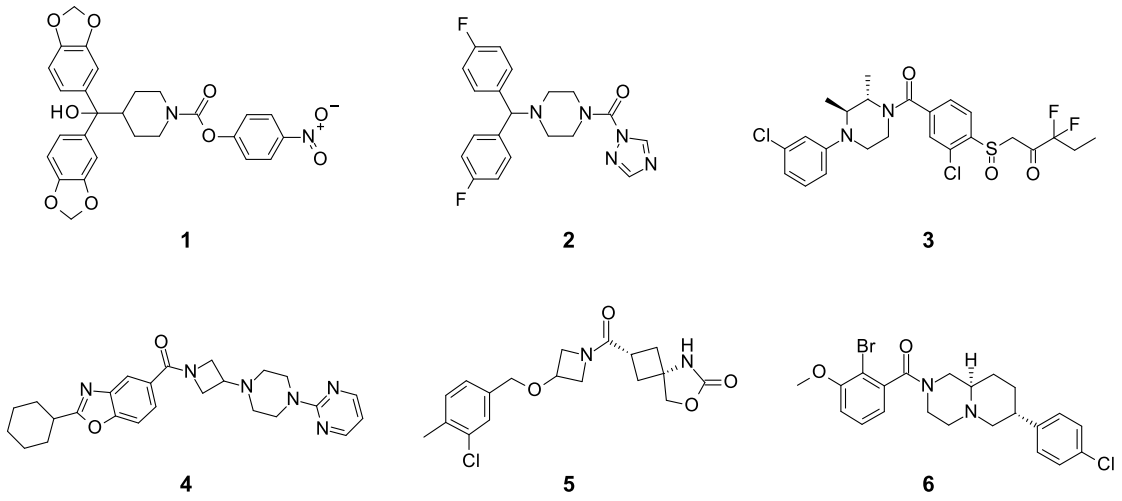

Figure 1. Selected MAGL inhibitors.

production.[15,16] Acute pharmacological blockade or genetic inactivation of MAGL in mice increases the levels of 2-AG and concomitantly reduces the AA concentration. In $Mgll^{-/-}$ mice, 2-AG brain levels increase, e.g., by ∼10-fold, reflecting a near 90% decrease in the rate of 2-AG degradation.[17] Due to the pivotal role of MAGL in the regulation of both eCB and eicosanoid signaling, MAGL inhibition has emerged as a promising therapeutic strategy for a range of brain disorders including (neuro) inflammatory and neuropsychiatric diseases, as well as conditions involving acute tissue injury and cancer.[18−21] MAGL inhibitors were efficacious in multiple preclinical models of neuropathic pain, encompassing models of traumatic nerve injury and chemotherapy-induced peripheral neuropathy, and multiple sclerosis via cannabinoid CB_1 and CB_2 receptor mechanisms.[21−23] First-generation MAGL inhibitors[24−26] act irreversibly by forming a covalent bond with the catalytic Ser122 residue of MAGL.[27] Chronic exposure to irreversible MAGL inhibitors can, however, result in unwanted CNS-mediated side effects. JZL-184 (Figure 1, **1**) induced pharmacological tolerance, physical dependence, impaired synaptic plasticity, and CB_1R desensitization in the CNS of rodents, reflecting prolonged exposure to high levels of 2-AG.[28] Furthermore, the irreversible MAGL inhibitor Lu-AG06466 was evaluated in a phase 2 clinical trial in patients with Tourette syndrome reporting mild to moderate adverse events.[29] In addition, irreversible hydrolase inhibitors may lack selectivity if the reactivity of the warhead and the decoration of the pharmacophore are not sufficiently optimized. This can lead to adverse effects that can be fatal in some cases.[30] Therefore, the development of highly selective reversible MAGL inhibitors is thought to improve the pharmacological control of enzyme activity and hence reduce the risk for off-target and adverse effects.

Different types of MAGL inhibitors have been developed, and the state of the art has been summarized in recent reviews.[31−33] Many of these molecules are covalent irreversible inhibitors containing an activated carbamate or urea motif attached to different leaving groups (compounds **1**−**2** in Figure 1). Examples for this are the early tool compound JZL-184 (**1**), SAR629 (**2**) for which the first MAGL cocrystal structure was determined,[34] the clinical MAGL inhibitor Lu-Ag06466,[35] PF-06795071,[36] and azetidinone-based irreversible inhibitors from the Butini group.[37] Recently discovered LEI-515 (**3**) is a peripherally restricted covalent reversible inhibitor containing an α-CF_2 ketone warhead.[21,38] Several noncovalent inhibitors have also been identified in recent years; however, they typically suffer from only modest MAGL potency or contain structural liabilities.[39−48] Exceptions to this are azetidinyl amide **4** from Janssen, which was also the first reversible inhibitor cocrystallized with MAGL,[49] and inhibitors from Takeda featuring a piperazinyl pyrrolidin-2-one core.[50] Recent cyclobutane-carbamate **5**[51] and bicyclopiperazine **6**[52] demonstrated in vivo target engagement by dose-dependently modulating 2-AG and AA rodent brain levels and stimulated the discovery of further optimized MAGL inhibitors with favorable drug-like properties.

Our focus of this work was on identifying novel reversible MAGL inhibitors with high potency and selectivity for the target as well as excellent absorption, distribution, metabolism, and excretion (ADME) properties. We employed a focused screening approach, followed by structure-guided medicinal chemistry optimization.

RESULTS AND DISCUSSION

To identify novel MAGL inhibitors, we performed a focused screen of a subset of the Roche compound library. The library selection process relied on a combination of three approaches: (a) a diverse subset of ∼51k compounds with lead-like properties from the Roche screening collection, (b) a focused subset of ∼18.5k molecules based on several complementary computational methods, and (c) a diverse subset of ∼1.6k compounds from a previous internal project targeting a different lipase (Figure 2). The focused subset included 2D fingerprint and graph similarity as well as 3D shape similarity to reference inhibitors, complemented by pharmacophore and docking searches using crystal structure information. The final library of ∼71.1k compounds was screened in an enzymatic assay based on the hydrolysis of 4-nitrophenylacetate by MAGL and yielded 2398 hits with IC_{50} < 10 μM (hit rate: 3.4%).

The number of hits identified by each method and their respective hit rates are summarized in Table S1. All methods contributed to the hits with individual hit rates ranging from 2 to 5%. The high number of hits suggests generally high druggability of the MAGL binding site. Interestingly, the target-agnostic diversity selection also showed a high hit rate.

https://doi.org/10.1021/acs.jmedchem.4c01769
J. Med. Chem. 2024, 67, 18448−18464

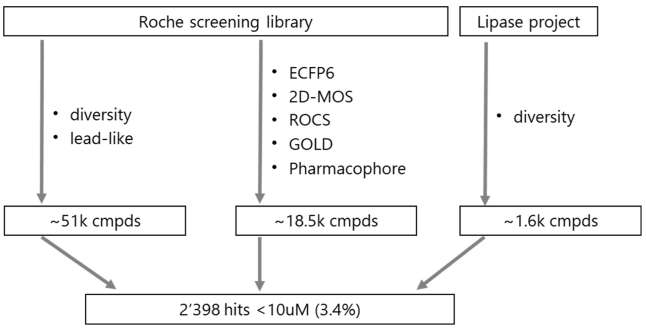

Figure 2. Library design for the focused screen. Details of the computational methods are provided in the Experimental Section.

However, as was found out later in the hit validation process, several of the compounds identified in this subset inactivated MAGL by undesired irreversible inhibition.

The benzoxazinone screening hit **7a** (Table 1) attracted our attention due to its high ligand efficiency (LE) of 0.38. It inhibits MAGL with an IC_{50} of 75 nM. Soon after the discovery of this hit, we were able to determine an X-ray crystal structure of this compound with human MAGL (Figure 3), which further guided our optimization efforts. The cocrystal structure confirmed noncovalent binding to MAGL in which the central amide is located on top of the catalytic Ser122. Its carbonyl oxygen atom is engaged in hydrogen bonding interactions in the oxyanion hole with the backbone NH donors of Ala51 and Met123, respectively. All three polar atoms of the benzoxazinone moiety are engaged in hydrogen

Table 1. Benzoxazinone Focused Screening Hit 7a and Early Optimizations of This Class

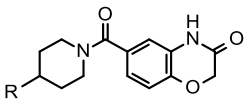

Compound	R	MAGL inh. (IC_{50}, μM)[a]	MAGL pIC_{50} ± SD[b]	LE[c]	logD[d]	Solubility[f] [μg/mL]
7a		0.075	7.13 ± 0.08	0.38	3.2	1.1
7b	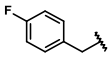	0.062	7.24 ± 0.17	0.37	3.3	0.8
7c	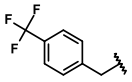	0.032	7.54 ± 0.24	0.34	3.8	4.1
7d		0.051	7.31 ± 0.12	0.37	3.6	36
7e	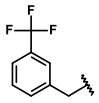	0.046	7.35 ± 0.09	0.34	3.9	15
7f	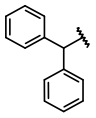	0.0005	9.36 ± 0.15	0.40	3.8	<0.1
7g	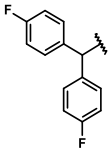	0.0009	9.19 ± 0.35	0.37	3.8[e]	<0.1
7h	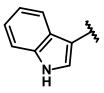	0.037	7.51 ± 0.27	0.36	2.9	37
7i	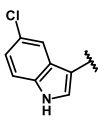	0.003	8.59 ± 0.33	0.40	3.6[e]	2
7j	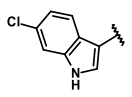	0.021	7.86 ± 0.40	0.36	3.8	0.3

[a]Rapidfire MS native substrate assay on purified human MAGL enzyme ($n \geq 3$, values are means).[53] [b]Negative decadic logarithm of MAGL inhibition IC_{50} values including standard deviation (SD). [c]LE stands for ligand efficiency. [d]Octanol/water distribution coefficient at pH 7.4. [e]Predicted log *D* based on internal machine-learning model. [f]Aqueous solubility at pH 6.5 in 0.05 M phosphate buffer.

https://doi.org/10.1021/acs.jmedchem.4c01769
J. Med. Chem. 2024, 67, 18448−18464

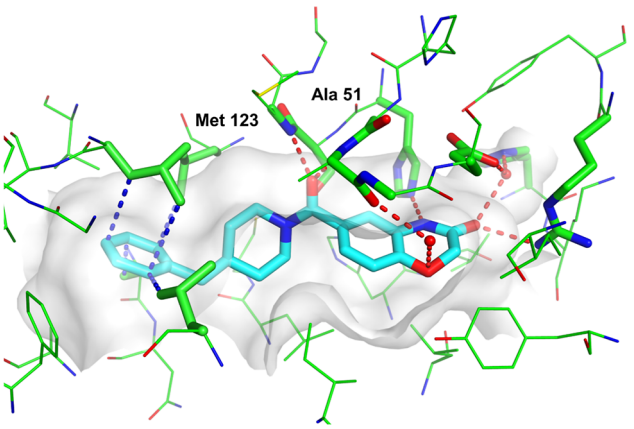

Figure 3. Co-crystal structure of human MAGL (green) with focused screening hit **7a** (cyan, pdb code: 9F8A). Residues of the oxyanion hole (Ala51 and Met123) which are on top of the catalytic Ser122 are labeled. Hydrogen bonds between the ligand and the protein or water are shown as red, dashed lines. Dispersion interactions with short distances (<4.0 Å) in the hydrophobic pocket on the left are highlighted as blue lines. Water molecules are removed except for the ones that form hydrogen bonds with the ligand.

bonds with the protein, either directly or through water mediation. A hydrophobic pocket formed by several aliphatic residues is apparent around the terminal phenyl group, and several close intermolecular carbon−carbon interactions can be identified. An overlay of our focused screening hit with the X-ray cocrystal structures of **4** and the covalent irreversible inhibitor **2**, respectively, revealed interesting commonalities and differences (Figure S1). All three inhibitors occupy the hydrophobic pocket in which the benzyl group resides, suggesting a binding hot-spot in MAGL. The central amide groups of **4** and our inhibitor series nicely overlap and are engaged in identical hydrogen bonding interactions in the oxyanion hole. In contrast to the noncovalent inhibitor **4**, our screening hit does not protrude into the induced fit pocket generated by the piperazinyl pyrimidine fragment.

Based on the X-ray structure analysis, we hypothesized that we could enhance the binding by improved filling of the hydrophobic region around the terminal benzyl group. Indeed, substitution by fluorine or trifluoromethyl, especially at the *para*-position, led to a gain in MAGL inhibitory activity compared to the original screening hit **7a** (Table 1). Branching off of the methylene linker by another phenyl ring, as suggested by the overlay with the irreversible inhibitor **2** (Figure S1, top), yielded compounds with subnanomolar MAGL IC_{50} values and with even increased LEs of 0.40 (compound **7f**). A very potent replacement of the original benzyl moiety was 3-substituted indole groups. Attaching an additional chlorine atom in the 5-position resulted in compound **7i** with IC_{50} = 3 nM and LE = 0.40. The cocrystal structure of this compound with MAGL shows many favorable dispersion interactions of the Cl substituent in a hydrophobic pocket (Figure S2).

These limited optimization efforts resulted in very potent MAGL inhibitors with promising early ADME profiles including good solubility (cf. **7d** and **7h** with an aqueous solubility of 36 and 37 μg/mL, respectively) and exhibiting a

Table 2. Head Group Replacements

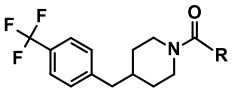

Compound	R		MAGL inh. (IC_{50}, μM)[a]	MAGL $pIC_{50} \pm SD$[b]	LE[c]	logD[d]	Solubility[f] [μg/mL]
7c	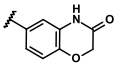		0.032	7.54 ± 0.24	0.34	3.8	4.1
7k	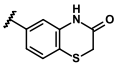		2.5	5.62 ± 0.11	0.26	3.7[e]	6.9
7l	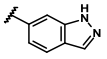		0.965	6.04 ± 0.14	0.29	3.8[e]	2.9
7m	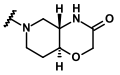	and enantiomer	0.370	6.46 ± 0.17	0.30	3.2	78
7n	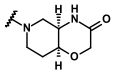	and enantiomer	0.065	7.22 ± 0.17	0.33	3.2	225
7o	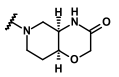		0.032	7.55 ± 0.22	0.34	3.3	231
7p	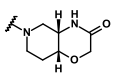		2.2	5.65 ± 0.04	0.26	3.3	114
7q	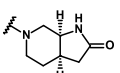	or enantiomer	0.569	6.30 ± 0.24	0.30	3.2	377

[a]Rapidfire MS native substrate assay on purified human MAGL enzyme ($n \geq 3$, values are means).[53] [b]Negative decadic logarithm of MAGL inhibition IC_{50} values including standard deviation (SD). [c]LE stands for ligand efficiency. [d]Octanol/water distribution coefficient at pH 7.4. [e]Predicted log *D* based on the internal machine-learning model. [f]Aqueous solubility at pH 6.5 in 0.05 M phosphate buffer.

https://doi.org/10.1021/acs.jmedchem.4c01769
J. Med. Chem. 2024, 67, 18448−18464

high propensity to reach the brain as they are no substrates of the P-glycoprotein transporter (cf. human P-glycoprotein efflux ratios[54] of 1.1, 1.2, and 1.2 for compounds **7e**, **7g**, and **7i**, respectively). To further improve on these properties, we investigated replacements of the benzoxazinone headgroup. We explored different ring systems with similar shapes trying to maintain the intermolecular hydrogen bonding pattern of the cyclic amide functionality in the reference compound (Figure 3). Table 2 summarizes MAGL IC_{50} values and selected ADME properties with different head groups. Replacement of the benzoxazinone of reference **7c** by benzothiazinone (**7k**) or indazole (**7l**) ring systems resulted in a >30-fold drop of inhibitory activity, with aqueous solubility remaining low. A breakthrough in solubility could be achieved by replacing the phenyl ring of the central benzamide by a saturated piperidine fragment. For example, the fully saturated hexahydro-pyrido-oxazinone (HHPO) **7n** had a 55-fold higher aqueous solubility compared to the analogous benzoxazinone **7c**.

Our initial choice of nitrogen-linked piperidine as bioisosteric replacement of a phenyl ring was motivated by a similar torsional preference around the bond to the amide carbonyl, which is a consequence of sp^2 conjugation. MAGL activities could be preserved in this way, with an equal IC_{50} for **7o** vs **7c**. Surprisingly, the racemic mixture of *trans*-HHPO isomer **7m**, which is more similar in shape to the benzoxazinone reference **7c** than the racemic mixture of *cis*-isomer **7n**, was ∼6-fold less potent. Chiral separation of the racemate **7n** yielded the two enantiomers **7o** and **7p**, which differed in their MAGL potency by 2 orders of magnitude. To better understand the reason for these activity differences, we determined cocrystal structures of human MAGL with *cis*- and *trans*-HHPO's **7n** and **7m**, respectively (Figure 4). For the *cis*-HHPO racemate, the 4*R*,8*S* isomer could be unambiguously identified from the electron density, which is the more active of the two *cis* stereoisomers. Although the *cis*-HHPO headgroup is more three-dimensional than the benzoxazinone, the positions of the central carbonyl in the oxyanion hole and the ring amide group overlap very well, with little changes in the protein conformation. The observed structure−activity relationship becomes clearer when performing quantum-mechanical (QM) conformational analyses on the ligands shown in Figure 4 (Figure S3). The two torsional angles connecting the central carbonyl group with the piperidine ring and headgroup, respectively, are key determinants for the shape of the ligand in a region where many hydrogen bonds can be formed with the protein. The QM results show that the preferred torsional angle between the carbonyl group and the headgroup differs by ∼30° when connecting to the benzoxazinone vs *cis*- or *trans*-HHPO moiety. Apparently, this shift of torsional preference can be better compensated by the *cis*-stereochemistry in the HHPO ring system, allowing for a similar positioning of the ring hydrogen bond donors and acceptors in comparison to the potent benzoxazinone headgroup. It should also be noted that the ring ether oxygen atom in the *cis*-HHPO group coordinates a water molecule in the binding site. Such an interaction is absent in the *trans*-HHPO crystal structure, in which the corresponding oxygen atom points into a lipophilic region. This is one of the small differences in the X-ray structure comparison, and we hypothesize that both the additional water contact and less ligand strain in positioning the ring polar atoms for hydrogen bond interactions contribute to the ∼6-fold better IC_{50} value of the *cis* isomer.

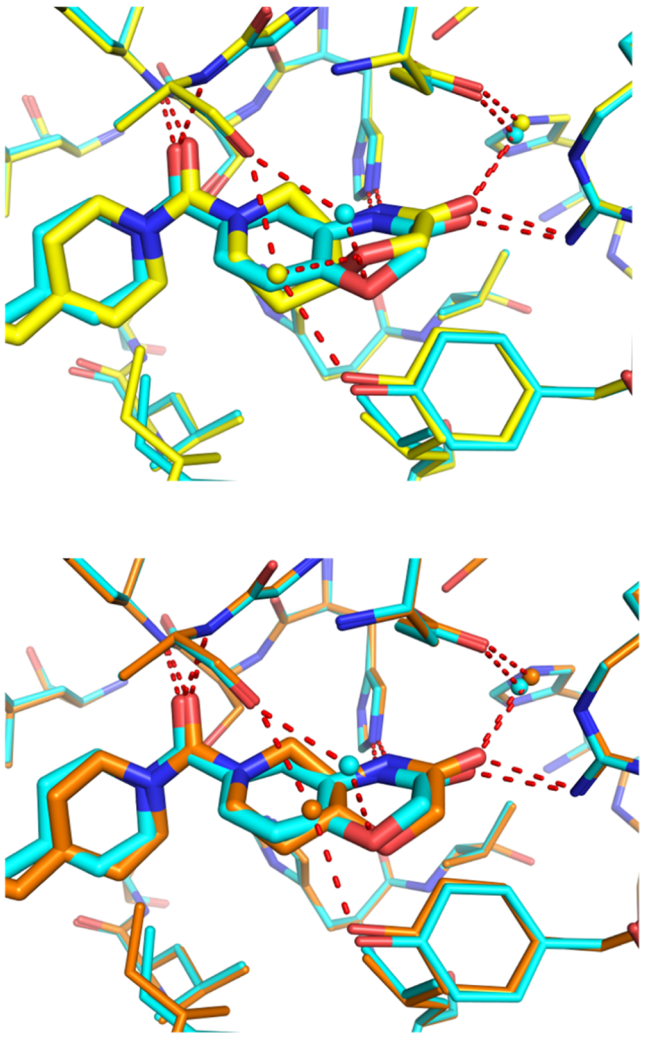

Figure 4. Top: overlay of cocrystal structures of human MAGL with benzoxazinone screening hit **7a** (cyan, PDB code: 9F8A) and with *cis*-HHPO **7n** (yellow, PDB code: 9F8B). Based on the electron density, a single enantiomer with a *cis*-(4*R*,8*S*) configuration can be unambiguously defined, which we attribute to the structure **7o**. Bottom: overlay of cocrystal structures of human MAGL with benzoxazinone screening hit **7a** (cyan, PDB code: 9F8A) and with *trans*-HHPO **7m** (orange, PDB code: 9F8C). Based on the electron density, a single enantiomer with *trans*-(4*R*,8*R*) configuration can be unambiguously defined. Water molecules are removed except for the ones that form hydrogen bonds with the head groups. Hydrogen bonds between the ligand and the protein or water are shown as red, dashed lines.

All HHPO stereoisomers (**7m**−**p**) and pyrrolidone **7q** exhibited significantly improved physicochemical properties compared to the corresponding benzoxazinone **7c**. Lipophilicity was lowered by approximately half a log unit. Solubility was tremendously improved with **7q** (377 μg/mL) being almost 2 orders of magnitude more soluble than **7c** (4.1 μg/mL). Interestingly, *cis*-HHPOs **7n**−**7p** were superior with regards to their solubility as compared to the *trans*-congener **7m**, which can likely be attributed to a more three-dimensional shape and better solvent exposure of the polar elements. The solubility of *cis*-HHPO **7o** was twice as high as that for its less potent congener **7p**. Furthermore, the change of the head group significantly improved the free fraction in human plasma, which was ∼9-fold higher for HHPO **7o** (4.3%)

https://doi.org/10.1021/acs.jmedchem.4c01769
J. Med. Chem. 2024, 67, 18448−18464

Scheme 1. Synthesis of Benzoxazinones 7a–j, Benzothiazinone 7k, and Indazole 7l[a]

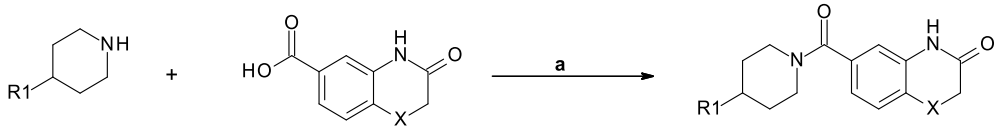

8a, R1 = Bn
8b, R1 = 4-F-Bn
8c, R1 = 4-CF_3-Bn
8d, R1 = 3-F-Bn
8e, R1 = 3-CF_3-Bn
8f, R1 = Ph_2CH
8g, R1 = 4-F-Ph_2CH
8h, R1 = 1*H*-Indol-3-yl
8i, R1 = (5-Chloro-1*H*-indol-3-yl)
8j, R1 = (6-Chloro-1*H*-indol-3-yl)

9a, X = O
9b, X = S

7a, R1 = Bn, X = O
7b, R1 = 4-F-Bn, X = O
7c, R1 = 4-CF_3-Bn, X = O
7d, R1 = 3-F-Bn, X = O
7e, R1 = 3-CF_3-Bn, X = O
7f, R1 = Ph_2CH, X = O
7g, R1 = 4-F-Ph_2CH, X = O
7h, R1 = 1H-Indol-3-yl, X = O
7i, R1 = (5-Chloro-1*H*-indol-3-yl), X = O
7j, R1 = (6-Chloro-1*H*-indol-3-yl), X = O
7k, R1 = 1*H*-Indol-3-yl, X = S

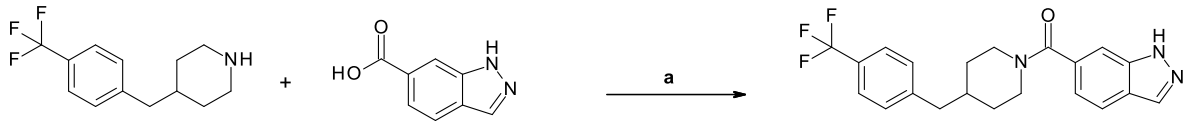

8c **10** **7l**

[a]Reagents and conditions: (a) HATU, DIPEA, DMF, rt; 18 h.

Scheme 2. Synthesis of HHPOs 7m–p and Pyrrolidone 7q[a]

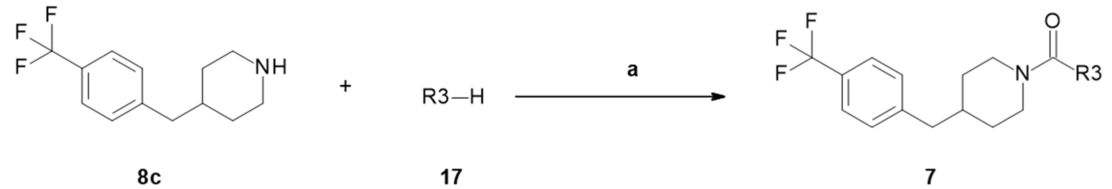

8c **17** **7**

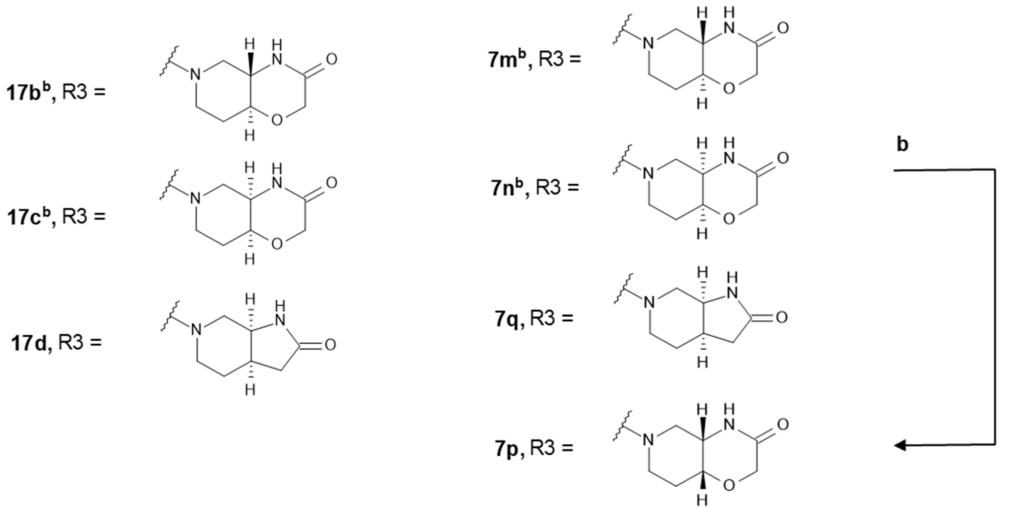

[a]Reagents and conditions: (a) (1) bis(trichloromethyl) carbonate, amine **17a–c**, $NaHCO_3$, DCM, 0 °C, 15 min, rt, 16 h, (2) DIPEA, 4-[[4-(trifluoromethyl)phenyl]methyl]piperidine, 0 °C, 15 min, rt, 2.75 h; (b) chiral separation of racemate **7n** on a Chiralcel-OD column using a gradient of *n*-heptane and EtOH containing 0.1% NH_4OAc. [b]Racemic mixture.

versus benzoxazinone **7c** (0.5%). Overall, *cis*-HHPO **7o** exhibited the most attractive profile and, therefore, was subject to more detailed investigations.

Benzoxazinones **7a–j**, the corresponding benzothiazinone **7k**, and indazole **7l** were synthesized from commercially available piperidines **8a–j** and commercially available carbox-

https://doi.org/10.1021/acs.jmedchem.4c01769
J. Med. Chem. 2024, 67, 18448–18464

Scheme 3. Asymmetric Synthesis of (4*aR*,8*aS*)-4*a*,5,6,7,8,8*a*-Hexahydro-4*H*-pyrido[4,3-*b*][1,4]oxazin-3-one 17a and Condensation toward Privileged HHPO 7o[a]

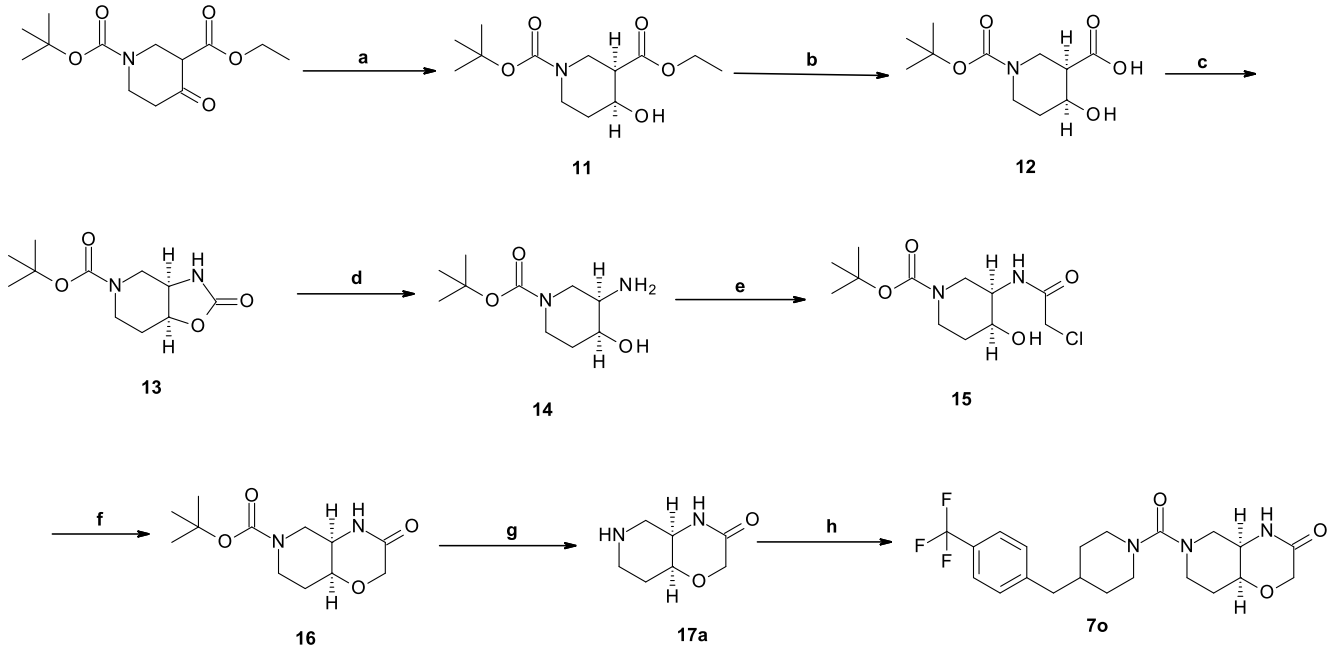

[a]Reagents and conditions: (a) ADH-74, GDH-105, NADP, D(+)-glucose, Kpi, $MgCl_2$, 2-PrOH, NaOH 1 M, rt, 19 h; (b) (1) NaOH 2 M, TBME, (2) HCl, rt, 1.5 h; (c) DPPA, Et_3N, toluene, 80 °C, 3 h; (d) NaOH 2 M, MeOH, 70 °C, 6.5 h; (e) chloroacetyl chloride, Na_2CO_3, toluene, water, 5 °C, 50 min; (f) KOH, 2-PrOH, 40 °C, 0.5 h; (g) (1) aqueous HCl 25%, 1-PrOH, 70 °C, 2 h, (2) NH_2Si column with MeOH/MeCN; and (h) 4-[[4-(trifluoromethyl)phenyl]methyl]piperidine **8c**, HATU, DIEA, DMF, rt, 18 h.

ylic acids **9a–b** and **10** using standard amide coupling conditions (Scheme 1).

HHPO-derived novel MAGL inhibitors **7m–p** and corresponding pyrrolidone **7q** were generated from commercial racemic HHPO building blocks **17b**, **17c**, and **17d**, respectively, through condensation with 4-[[4-(trifluoromethyl)phenyl]methyl]piperidine **8c** (Scheme 2). Chiral separation of racemic *cis*-HHPO **7n** allowed for accessing enantiomerically pure stereoisomers **7p** and **7o**. In analogy, the racemic product of **17d** was separated on a chiral column to obtain compound **7q**.

For accessing the enantiomerically pure *cis*-stereoisomer **7o** in larger quantities, a novel asymmetric synthesis using a dynamic kinetic resolution via an enzymatic ketoreduction as a key step toward **17a** was developed (Scheme 3). The synthesis commenced from commercial *rac*-1-(*tert*-butyl) 3-ethyl 4-oxopiperidine-1,3-dicarboxylate (CAS RN 98977-34-5) which was enantioselectively reduced by the alcohol dehydrogenase ADH-74 to exclusively provide the *cis*-isomer of piperidine **11** with 100% ee. Subsequent ester hydrolysis and Curtius rearrangement delivered carbamate **13** in a 66% yield over two steps. Enantiomerically pure *cis*-HHPO **17a** was accessed via carbamate hydrolysis, amidation of resulting amino alcohol **14** with chloroacetyl chloride, cyclization of intermediate **15** under basic conditions followed by removal of the Boc protecting group through acidic workup in 48% yield over four steps.

HHPO **7o** exhibited favorable physicochemical properties including high kinetic solubility (231 μg/mL) and a low lipid membrane binding assay (LIMBA) log D_{brain} of 1.8 which is supportive for a significant free fraction in brain tissue and thus important for neuroscience indications (Table 3).[54] Furthermore, MAGL inhibitor **7o** permeated well through membranes (PAMPA P_{eff} = 12.8 cm/s*10 × 10^{-6}) and was chemically stable at a pH range of 1 to 10 in aqueous buffer systems.

Table 3. Physicochemical Properties of HHPO 7o

MW [g/mol]	425.45
PSA [Å^2]	55
solubility[a] [μg/mL]	231
log D[b]	3.3
LIMBA log D_{brain}[c]	1.8
PAMPA P_{eff} [cm/s*10 × 10^{-6}][c]	12.8
chemical stability in aqueous buffer	stable at pH 1, 4, 6.5, 8, and 10 for 2 h at 37 °C

[a]Aqueous solubility at pH 6.5 in 0.05 M phosphate buffer. [b]pH 7.4. [c]See the Experimental Section.

To assess the suitability of running in vivo target engagement and pharmacodynamics studies in animal models, **7o** was investigated for its potency on mouse, rat, and cynomolgus monkey MAGL. For all species, consistent double-digit nanomolar activity was observed (Table 4). The binding kinetics of HHPO **7o** was examined using the surface plasmon resonance (SPR) assay. The ligand binds noncovalently to the immobilized MAGL proteins in SPR real-time monitoring. Equilibrium dissociation constants (K_d) were 45 and 64 nM for human and rat MAGL, respectively. Association and dissociation rate constants (k_{on}, k_{off}) of the ligand–enzyme complex indicated fast association and dissociation behavior of the inhibitor. HHPO **7o** was tested against a customized panel of 50 representative off-targets,[55] exhibiting an excellent selectivity profile (Table S2). Selectivity against other hydrolases including structurally and functionally similar serine hydrolases such as ABHD6, ABHD12, FAAH, and DAGL was

https://doi.org/10.1021/acs.jmedchem.4c01769
J. Med. Chem. 2024, 67, 18448–18464

Table 4. In Vitro Pharmacology Data of HHPO 7o

human/mouse/rat/cyno MAGL inhibition IC_{50} [nM][a]	32/91/71/16
human/rat MAGL SPR K_d [nM][b]	45/64
human/rat MAGL SPR	2.5×10^5/2.6×10^5
k_{on} [1/M/s]/k_{off} [1/s]	7.5×10^{-3}/16.8×10^{-3}
off-target panel screen against 50 representative proteins at 10 μM[c]	inhibition <50% except for serotonin transporter (57%)
hydrolase selectivity in gel-based ABPP assay at 10 μM[d]	no off-targets

[a]Rapidfire MS native substrate assay on purified human, mouse, rat and cynomologus monkey MAGL enzyme ($n \geq 3$ for human, mouse and rat MAGL, values are means; $n = 1$ for cynomologus monkey MAGL).[53] [b]Experimental Section. [c]See Table S2. Off-target data were generated at Eurofins Cerep (France). [d]See Figure S4. ABPP selectivity data were generated as previously reported.[56]

assessed using a previously reported multiplex activity-based protein profiling (ABPP) assay in mouse brain proteome[56] (see Figure S4). Importantly, HHPO **7o** demonstrated remarkable specificity and selectivity, exclusively blocking MAGL, with no other potential off-target activity detectable at a concentration of 10 μM.

Due to its favorable potency, selectivity, and physicochemical properties, MAGL inhibitor **7o** was further investigated for its ADME profile. It showed high stability in microsomal clearance assays, which translated also into good hepatocyte stability (Table 5). As a consequence of its increased three-dimensionality, HHPO **7o** exhibited increased fractions unbound being >3% in all tested species as compared to its benzoxazinone congener **7c** (fraction unbound in human plasma protein 0.5%). Importantly, **7o** demonstrated high permeability in the P-glycoprotein (P-gp) efflux transporter assay (human $P_{app,\ AB\ inhibitor}$ = 176.4 nm/s and mouse $P_{app,\ AB\ inhibitor}$ = 243.8 nm/s, respectively). Due to the high intrinsic permeability, it was expected to enter the brain despite being a weak P-gp substrate, which was confirmed in PK studies with racemic *cis*-HHPO **7n** and enantiomerically pure **7o** in mice and rats, respectively (Table 5). The total brain-to-plasma ratio of **7n** following i.p. administration (24 mg/kg) in mice was 1.7, and the unbound brain (approximated by CSF concentrations) to unbound plasma (factoring in plasma protein binding) ratio ($K_{p,uu}$) was 0.35, i.e., approximately one-third of free systemic plasma concentrations. This difference was expected due to the aforementioned weak P-gp substrate properties. Overall, **7n** showed a very favorable in vivo mouse PK profile with low clearance and high bioavailabilities after both i.p and p.o. administration, rendering it well suited for in vivo target engagement studies. In vivo clearance of HHPO **7o** in rats was around 10% of the liver blood flow (CL = 4.6 mL/min/kg). Together with a moderate volume of distribution (V_{ss} = 1.3 L/kg) and a terminal half-life of 5.1 h, the molecule exhibited a good rat PK profile. After p.o. and i.p. administration, excellent exposures and complete bioavailability were obtained. Furthermore, the data indicated a very fast absorption and after i.p. administration, a total brain-to-plasma ratio around 1 and a $K_{p,uu}$ value of 0.53, again indicating good CNS exposure. Importantly, no behavioral side effects were observed despite high brain exposures in the rodent PK studies, thus making HHPO **7o** a suitable candidate for interrogating MAGL pharmacology in a disease setting.

Table 5. ADME and Rat PK Profile of MAGL Inhibitor 7o as well as Mouse PK Profile of the Racemic Mixture 7n

human/mouse/rat clearance in microsomes [μL/min/mg protein][a]	<10[b]/<10[b]/11
human/mouse/rat clearance in hepatocytes [μL/min/10 × 10^6 cells][c]	1.9/8.9/4.0
human/mouse/rat plasma protein binding [%][d]	4.3/4.7/3.2
human/mouse P-glycoprotein efflux ratio[d]	2.4/4.0
$P_{app,\ AB\ inhibitor}$ [nm/s]	176.3/243.9
mouse PK profile[e]	
CL [mL/min/kg] (i.v.)	23
V_{ss} [L/kg] (i.v.)	3.0
$T_{1/2}$ [h]	1.5 (i.v.)/2.9 (i.p.)
C_{max} [ng/mL]	896 (p.o.)/12,200 (i.p.)
T_{max} [h]	2.7 (p.o.)/1.5 (i.p.)
AUC_{last} [h*ng/mL]	4560 (p.o.)/62,100 (i.p.)
F [%]	127 (p.o.)/368 (i.p.)
brain/plasma ratio (average)	1.7 (i.p.)
CSF/plasma ratio (average); $K_{p,uu}$	0.0164 (i.p.); 0.35
rat PK profile[f]	
CL [mL/min/kg] (i.v.)	4.6
V_{ss} [L/kg] (i.v.)	1.3
$T_{1/2}$ [h]	5.1 (i.v.)/2.7 (i.p.)
C_{max} [ng/mL]	1290 (p.o.)/12,200 (i.p.)
T_{max} [h]	6.0 (p.o.)/0.25 (i.p.)
AUC_{last} [h*ng/mL]	19,100 (p.o.)/40,200 (i.p.)
F [%]	115 (p.o.)/111 (i.p.)
brain/plasma ratio (average)	1.1 (i.p.)
CSF/plasma ratio (average); $K_{p,uu}$	0.017 (i.p.); 0.53

[a]Microsomal clearance data were generated as previously reported by our group.[53] [b]The clearance rate was below the assay sensitivity range. [c]Hepatocyte clearance data were generated as previously reported by our group.[57] [d]See the Experimental Section. [e]In vivo pharmacokinetics of racemic *cis*-HHPO **7n** in mice following a 1.3 mg/kg i.v., 5.1 mg/kg p.o., and 24 mg/kg i.p. administration, respectively. [f]In vivo pharmacokinetics of *cis*-HHPO **7o** in rats following a 1 mg/kg i.v., 5 mg/kg p.o., and 10 mg/kg i.p. administration, respectively. CL, clearance; F, bioavailability; V_{ss}, volume of distribution; and $K_{p,uu}$, unbound brain-to-plasma partition coefficient.

Prior to running in vivo target engagement studies, in vitro safety assessments were conducted with MAGL inhibitor **7o**. No risk of drug−drug interactions was observed as **7o** did not inhibit the three most important cytochrome P450 isoenzymes (Table 6). Furthermore, no glutathione adducts, which would point to the formation of reactive metabolites, were detected, and only a weak interaction with the human Ether-à-go-go-related gene (hERG) ion channel[58] was observed, which is not expected to trigger undesired cardiac effects. Finally, the

Table 6. In Vitro Safety Profile of MAGL Inhibitor 7o

CYP inhibition@10 μM (3A4/2C9/2D6) [%][a]	−195/3/−12
GSH (human liver microsomes) adducts[b]	none detected
hERG IC_{50} [μM][c]	7.7
Ames/MNT/phototoxicity	all negative

[a]CYP assays were conducted as previously described.[59] [b]GSH adduct formation data were generated as previously described.[60] [c]hERG inhibition data were generated as previously described.[61] CYP, cytochrome P-450; GSH, glutathione; and hERG, human ether-à-go-go-related gene.

https://doi.org/10.1021/acs.jmedchem.4c01769
J. Med. Chem. 2024, 67, 18448−18464

A

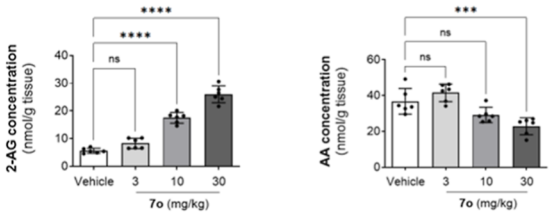

C

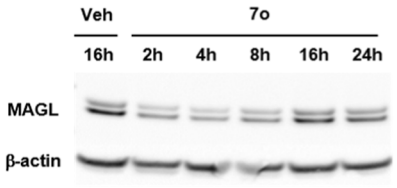

B

Dose (mg/kg)	Measured average plasma conc. (nM)	Calculated CSF conc. (nM)	Calculated % target occupancy
3	1901	31.2	49
10	7496	123	79
30	27765	455	93

D

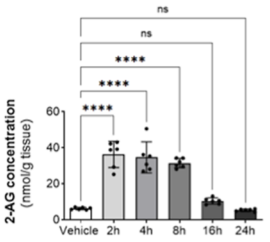

E

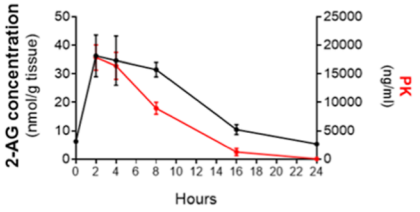

F

Time (h)	Measured average plasma conc. (nM)	Calculated CSF conc. (nM)	Calculated % target occupancy
2	42040	689	96
4	38588	633	95
8	21089	346	92
16	2955	48	60
24	100	2	5

G

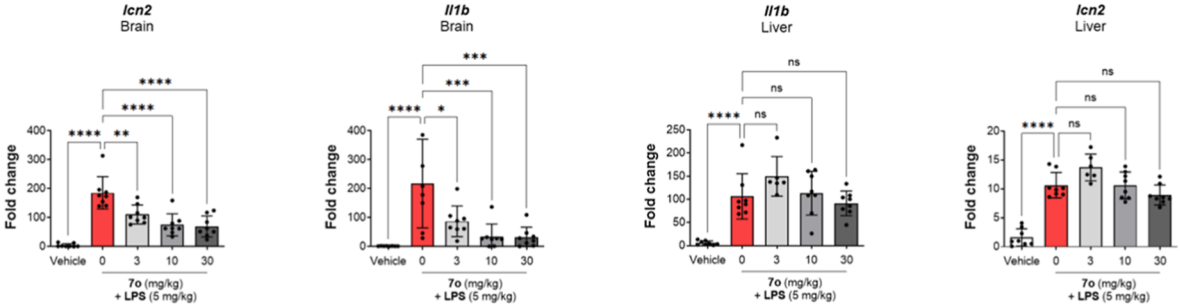

Figure 5. (A,B) Acute target engagement study performed with HHPO **7o** dosed at 3, 10, and 30 mg/kg. 2-AG and AA levels were measured in brain extracts by LC/MS 4 h post ip injection of the compound. Inlet table B shows the corresponding average plasma concentrations, calculated CSF concentrations (based on average CSF/plasma ratio of 0.0164), and calculated % target occupancy values (based on IC_{50} of 32 nM). (C) MAGL target occupancy determination using ABPP on the brain proteome of mice dosed with HHPO **7o**. Proteomes were prepared at the indicated time points. Maximum occupancy was visible at 2 h post compound administration. (D,F) Acute target engagement study performed with 30 mg/kg administered via the i.p. route of HHPO **7o** to evaluate 2-AG levels in the brain within a 24 h time period. Graph in part E shows the PK/PD correlation. Inlet table F shows the corresponding average plasma concentrations, calculated CSF concentrations, and calculated % target occupancy values (as described in B). (G) Efficacy of HHPO **7o** in the LPS model of neuroinflammation. Mice were dosed with vehicle, LPS or LPS + HHPO **7o** (3, 10, 30 mg/kg i.p.). mRNA analyses of LCN2 and Il1b demonstrated the anti-inflammatory properties of HHPO **7o** specifically in the brain.

compound did not show activity in the in vitro Ames and micronucleus test (MNT) genotoxicity assays nor in the in vitro 3T3 phototoxicity assay.

To investigate the in vivo potential of HHPO **7o**, vehicle (NaCl/DMSO/TW80 [80/10/10]) or the inhibitor, which was completely dissolved in a vehicle consisting of equal parts of DMSO and TW80 and diluted in 8 parts normal saline (NaCl/DMSO/TW80 [80/10/10]), was administered i.p. at 3, 10, and 30 mg/kg to mice. After 4 h, animals were sacrificed, and a dose-dependent increase of brain 2-AG and a decrease of AA levels were observed, thereby demonstrating target modulation of **7o** despite being a mouse P-gp substrate (Figure 5A). **7o** exposures increased approximately linearly reaching a calculated target occupancy of 79% at 10 mg/kg and almost complete occupancy at 30 mg/kg (Figure 5B). Subsequently, we performed a time course experiment monitoring brain 2-AG levels over 24 h after a 30 mg/kg i.p. injection. 2-AG levels were maximal after 2 h, started to decline after 8 h, and returned to basal levels after 24 h (Figure 5D). An ABPP experiment performed on brain proteome of mice dosed with 30 mg/kg of **7o** confirmed the highest MAGL occupancy at 2 h post-compound administration, which returned toward baseline (e.g., vehicle condition) from 16 h post-compound administration, correlating with plasma exposure (Figure 5C). Importantly, plasma exposure and calculated brain target occupancy levels were in line with brain

https://doi.org/10.1021/acs.jmedchem.4c01769
J. Med. Chem. 2024, 67, 18448−18464

2-AG levels, indicating a relationship of CSF exposure with target engagement (Figure 5E,F). Next, we evaluated the anti-inflammatory properties of **7o** in a lipopolysaccharide (LPS) model of neuroinflammation. CD-1 mice where dosed with NaCl + vehicle, LPS + vehicle, or LPS + **7o** (30 mg/kg i.p.) and sacrificed 6 h after compound administration.[52] Expression of LCN2 and IL1b, two markers of neuroinflammation,[62,63] were measured by droplet digital qRT-PCR in cortical brain lysates of dosed mice. **7o** significantly prevented LPS-induced mRNA expression of both pro-inflammatory markers specifically in the brain but not in peripheral tissue (Figure 5G), thus demonstrating the anti-inflammatory properties of our reversible MAGL inhibitor **7o**.

SUMMARY AND CONCLUSIONS

On the search for novel reversible MAGL inhibitors combining high potency and selectivity for the target with excellent ADME properties, we started out from a focused screening approach on a Roche library subset of ∼71.5k compounds. The library, which was composed of a diverse subset with lead-like properties, a selection based on diverse ligand- and structure-based computational methods, and a lipase-targeting subset, yielded 2398 hits with IC_{50} < 10 μM, which corresponded to an excellent hit rate of 3.4%. Benzoxazinone screening hit **7a** was of particular interest as it reversibly inhibited MAGL with an IC_{50} of 75 nM and showed a high LE of 0.38. The X-ray cocrystal structure with human MAGL confirmed the non-covalent interaction with the enzyme and enabled structure-guided optimization efforts. In the first round of optimization, the inhibitory potency of the ligands against MAGL could be improved by enhanced protein interactions in a hydrophobic region around the terminal benzyl group. While this led to very potent MAGL inhibitors, the ligands did not exhibit optimal ADME profiles yet. Increasing the carbon sp^3 content by replacing the original benzoxazinone headgroup with a *cis*-(4*R*,8*S*) hexahydro-pyrido-oxazinone moiety was key to improving ADME properties. Interestingly, a similar benzoxazinone screening hit was found previously by Ikeda et al. but then optimized toward a spiro headgroup.[51] Furthermore, Hao et al. recently reported benzoxazinone analogues as MAGL inhibitors, exhibiting moderate in vivo target engagement.[64]

A novel asymmetric synthesis using a dynamic kinetic resolution as a key step was developed to access the key HHPO building block **17a** and subsequent condensation with 4-[[4-(trifluoromethyl)phenyl]methyl]piperidine provided compound **7o**. This molecule is a very potent MAGL inhibitor across species with a fast target kinetics and is highly selective against common off-targets and brain hydrolases. HHPO **7o** matches the target compound profile for treating CNS diseases. This includes low lipophilicity, high solubility and permeability, and low human P-gp efflux. Excellent in vitro safety properties add further value to this MAGL inhibitor. Low microsomal and hepatocyte clearance translated to favorable mouse and rat PK profiles reaching high CSF exposures following ip and po administration despite some P-gp efflux in rodents. The combination of excellent in vitro potency and drug-like CNS ADME properties makes **7o** one of the best reported reversible MAGL inhibitors. Its superior property profile translated to in vivo target engagement in mouse brains, where a significant 2-AG increase was found already at ∼60% calculated target occupancy (based on CSF-concentrations and CSF/plasma ratios established in previous PK studies) following the acute administration of 15 mg/kg of **7o**. Furthermore, brain AA levels were dose-dependently lowered, and a time course experiment demonstrated the correlation of brain 2-AG level increase with plasma exposure. Importantly, these target engagement data translated into a significant reduction of brain IL-1β and LCN2 mRNA expression levels, both being critically involved in neuroinflammatory processes. In summary, the novel, highly potent, and selective reversible MAGL inhibitor **7o** shows a very favorable target compound profile and holds great promise for the treatment of neuroinflammatory and neurodegenerative diseases. The value of the reported *cis*-(4*R*,8*S*) HHPO series has already been further demonstrated by us using radiolabeled analogues in positron emission tomography (PET) studies of MAGL target engagement.[57,65]

EXPERIMENTAL SECTION

Selection of Focused Screening Library. The library used for the focused screen consisted of a preplated diverse subset of the Roche library with lead-like properties (50,960 compounds), a diversity selection of 1643 compounds from a previous internal lipase project, and a focused subset of 18,530 compounds based on several ligand- and protein structure-based computational approaches (Figure 2). Specifically, the latter included:

- Ligand-based two-dimensional ECFP6 (extended connectivity fingerprints, diameter of bond distance is 6)[66] similarity searches using key compounds from existing MAGL patents as references (1010 compounds)
- Ligand-based two-dimensional graph-based MOS (maximum overlapping spheres)[67] similarity searches using the non-covalent inhibitor **4** (Figure 1) as reference (1241 compounds)
- Three-dimensional shape-based similarity searches with ROCS,[68] again using **4** as reference (3997 compounds)
- MOE pharmacophore searches based on the MAGL-compound **4** cocrystal structure (PDB code 3PE6)[49] resulting in 9455 molecules
- GOLD docking runs against the MAGL protein structure of PDB code: 3PE6 (2827 compounds)
- Compounds identified by the individual methods were typically filtered further for hit-like properties and clustered to enable a diversity selection.

Crystallography. *Purification of Human MAGL.* Human MAGL with the sequence 1−303 containing amino acid variations K26A, L169S, L176S[49] was purified via His-tag and final size exclusion chromatography in buffer 50 mM HEPES pH 7.5, 200 mM NaCl, 2 mM DTT, 2 mM EDTA, and 2% glycerol.

Crystallization of Human MAGL and Soaking of Compounds. Human MAGL at a concentration of 10.7 mg/mL was incubated with ligand in three-fold molar excess overnight at 4 °C. Prior to crystallization experiments, the protein solution was centrifuged at 20,000*g*. Crystallization droplets were set up at 21 °C by mixing an aliquot of 0.1 μL of protein solution with 0.1 μL of crystallization screen solution (ProComplex Screen, Qiagen) in vapor diffusion sitting drop plates. Microcrystals were obtained out of 0.1 M HEPES, pH 7, 10% (w/v) PEG 4000, and 10% (v/v) isopropanol and subsequently used as seed crystals. Cross-seeding experiments yielded large rectangular shaped crystals out of 0.1 M MES pH 6.5, 7% w/v PEG MME 5K, and 15% v/v isopropanol within 2 days after setup and grew to final size within 1 week. For soaking experiments crystals were incubated with 10 mM compound for 16 h. Prior to data collection, crystals were transferred to crystallization buffer supplemented with 15% ethylene glycol and cryo-cooled in liquid N_2. Diffraction data were collected using a PILATUS 6 M detector at beamline X10SA of the Swiss Light Source (Villigen, Switzerland).

Structure Determination and Refinement of Human MAGL with Compounds. Data were processed with XDS[69] and scaled with SADABS (BRUKER). The orthorhombic crystals belonging to the space group $C222_1$ diffract to resolutions of 1.56 to 1.40 Å. Structures

https://doi.org/10.1021/acs.jmedchem.4c01769
J. Med. Chem. 2024, 67, 18448−18464

were determined by molecular replacement with PHASER[70] using the coordinates of a previously published MAGL structure with pdb accession code 3PE6 as a search model. With programs from the CCP4 suite[71] and BUSTER[72] the coordinates obtained by molecular replacement were subsequently refined by rigid body and positional refinement. Difference electron density was used to place the ligand. Manual rebuilding of protein was done with COOT.[73] The asymmetric unit contains one MAGL molecule. Data collection and refinement statistics are summarized in Table S3.

MAGL Enzymatic Assays. For the focused screen, an enzymatic assay was used similar to the one described in the MAGL Inhibitor Screening Assay Kit (item no. 705192, Cayman chemical company). The assay is based on the hydrolysis of 4-nitrophenylacetate by MAGL resulting in 4-nitrophenol with an absorbance of 405−412 nm. The assay buffer used contained 50 mM Tris-HCl pH 7.5 (Gibco, 15567-027) and 1 mM EDTA (Sigma-Aldrich, 03690-100 mL). 4-Nitrophenylacetate (Sigma-Aldrich, N-8130) was dissolved in ethanol to give a 10 mM solution.

In the focused screen setup, 0.5 μL of 4 mM compound dilutions in 100% DMSO was plated in 384-well nanoaliquot sample plates (Weidmann Medical Technology AG). Prior to the enzymatic assay, the compounds were diluted to 80 μM with 24.5 μL of assay buffer containing 6.1% DMSO, yielding 1% DMSO in the enzymatic reaction. 5 μL of the prediluted compounds was transferred into a black 384-well assay plate with clear bottom (Corning 3655, nonbinding surface, nonsterile polystyrene) containing 15 μL of MAGL (2.6 nM in assay buffer, 1 nM final). After a thorough mix with a 384-well pipettor and 20 min incubation time at rt, 20 μL of the 4-nitrophenylacetate substrate (600 μM in assay buffer, 300 μM final) was added to the enzyme-compound mix. After another mix with the 384-well pipet, the reaction was allowed to incubate for 5 min at rt before reading absorbance at 405 nm on a Spectramax Paradigm microplate reader equipped with an absorbance cartridge. The absorbance was measured again after an incubation of 80 min at rt, and the slope was calculated for analysis using Genedata Screener software.

For the routine profiling of compounds, a Rapidfire MS native substrate assay on purified human MAGL enzyme was used, as described previously.[53]

SPR Measurements. SPR experiments were performed on the T200 SPR instruments (Cytiva, Uppsala, Sweden) at 18 °C in 10 mM HEPES, 150 mM NaCl, 0.05% P20, pH 7.4, and 50 μM EDTA supplemented with 1% (v/v) DMSO. Protein was immobilized via standard amino coupling without ethanolamine quenching. Binding assay was performed at a flow rate of 30 μL/min with five concentration single-cycle kinetics (max conc. One μM, 2-fold dilutions steps).

Determination of Distribution Coefficients (Log D). The distribution coefficient log D was determined in a water/1-octanol system by the CAMDIS method (CArrierMediated DIstribution System),[74] which is based on the classical "shake flask" method. The compound of interest was prepared as 10 mM stock solution in DMSO, and a fixed aliquot size of 14 μL was added to 1.4 mL of water containing 25 mM phosphate buffered at pH 7.4. The experiment continued with the accurate coating of a hydrophobic layer (0.45 μm PVDF membrane), which was fixed on the bottom of each well in a 96-well filter plate. Each membrane was impregnated with 4 μL of 1-octanol. The coated membrane was covered with a predefined volume of the prepared aqueous sample solution described above. The plate was then sealed and shaken for 1.5 h at 21 °C. During this time, the substance was distributed between the membrane impregnated with octanol and the buffer solution. After distribution equilibrium, the filter plate was placed in the autosampler of the LC/MS instrument so that the remaining sample concentration in the aqueous phase can be analyzed. This method was carried out at two different 1-octanol/water ratios: one with excess buffer (200 μL), and the other with a small volume of buffer (50 μL). In both cases, the volume of the octanol phase was 4 μL. For each analyte, both octanol/water ratios were applied and carried out in triplicates. The distribution coefficient for a given analyte was then calculated from the difference in concentrations in the aqueous phase with and without octanol-coating and the derived concentration ratio of the two phases.

Determination of Brain-Polar-Lipids/Water Distribution Coefficients (LIMBA Log D_{brain}). Compounds of interest were added to buffer (50 mM Tris·HCl/114 mM NaCl/pH 7.4) as DMSO stock solutions (10 mM), resulting in sample solutions of 25 μM and DMSO content of 0.25%/vol. The solutions were filtered (NUNC cat. no. 278752), and aliquots of the filtrate (V_{aq} = 50 μL) were transferred into an in-house made Teflon plate. In parallel, DIFI tubes (Weidmann Plastics Technology AG, Rapperswill, Switzerland, 23358) were coated with a defined volume of a microemulsion ($V_{emulsion}$ = 4 μL in quadruplicate) consisting of 2.7%/w of porcine brain polar lipids extract (Avanti Polar Lipids Inc., 141101P, CAS number 86088-88-2), buffer (10.8%/w), dodecane (27.0%/w), and 59.5%/w of a mixture of 2-propanol and 1-butanol (1/1 vol) and dipped into the aqueous drug solution. The assay kit was sealed and allowed to stand at room temperature for 8 h. The selected incubation time of 8 h was based on prior experiments showing that distribution equilibrium was achieved after this time. After removal of the DIFI tubes, the equilibrium drug concentration in the aqueous phase was analyzed by LC−UV/MS as described below. In parallel, a reference experiment was carried out in the same plate without microemulsion to obtain the initial aqueous drug concentration, C_{aq}^{0}. The log D_{BPL} (pH 7.4) value was obtained by mass balance according to

$$\log D_{BPL} = \frac{C_{aq}^{0} - C_{aq}^{eq}}{C_{aq}^{eq}} \cdot \frac{V_{aq}}{V_{emulsion}}$$

Drug concentrations in aqueous solutions were quantified using an Agilent 1290 Infinity HPLC-MS system (Agilent Technologies, CA, USA) equipped with a DAD detector and an API single quadruple mass spectrometer (Agilent 6140). An aliquot of each sample (4 μL) was injected onto a Kinetex XB 1.7 μm, 2.1 mm × 30 mm analytical column (Phenomenex, Germany, Part. no. 00A-4498-AN) operated at 60 °C. The mobile phase consisted of A (water) and B (acetonitrile), both containing 0.1%/vol formic acid. The gradient elution was performed with a flow rate of 1.0 mL/min as follows: initial 5%/vol B, 0−0.35 min linear gradient from 5%/vol B to 95%/vol B, 0.35−0.65 min 95%/vol B, and post time 0.5 min.

Determination of PAMPA Values. The parallel artificial membrane permeability assay (PAMPA) is a technique used to assess the passive permeability of substances. This method involves transferring substances from a donor compartment through a lipid-infused artificial membrane into an acceptor compartment. The permeability coefficient (P_{eff}) of the drug and the concentrations of the test compound in the donor and acceptor compartments are measured. In this assay, a 96-well microtiter plate filled with aqueous buffer solutions (pH 7.4) was used. This plate was covered with a microtiter filter plate, creating a sandwich-like structure. The hydrophobic filter material was preimpregnated by a lipid/oil/lipid trilayer.[75] The donor compartment was filled with 300 μL of sample solution in triplicate and with an initial sample concentration of 20 μM. The acceptor plate (filter plate) contained 200 μL of blank solution. In both cases, phosphate-buffered saline, 50 mM, pH 7.4, was used. The working solutions had a maximum DMSO content of 5%. The sandwich construct was then incubated without shaking for 18 h at 21 °C. After incubation, the test sandwich was carefully disassembled to analyze the reference, donor, and acceptor solutions using LCMS.

Determination of Solubility Values. Kinetic solubilities were determined using a high-throughput lyophilization solubility assay (LYSA). The starting point of the assay was a 10 mM stock solution in DMSO. After removing the DMSO by centrifugal vacuum evaporation, 0.05 M phosphate buffer at pH 6.5 was added, and the samples were sonicated. After being filtered, the solutions were analyzed by MS/MS and/or HPLC. A 4- to 7-point calibration curve was also prepared in order to calculate the solubility value.

Determination of P-gp Values. P-glycoprotein (P-gp), also known as multidrug-resistance protein 1 (MDR1), is one of the most extensively studied and well-characterized drug transporters. The P-gp

https://doi.org/10.1021/acs.jmedchem.4c01769
J. Med. Chem. 2024, 67, 18448−18464

assay evaluates the capability of test compounds to be transported across cells as P-gp substrates.[76] This assay employed transfected LLC-PK1 cells (porcine kidney epithelial cells sourced from The Netherlands Cancer Institute) that express either human or mouse P-gp. These cells were cultured on a 96-well semipermeable filter membrane plate, forming a polarized monolayer with tight junctions, effectively acting as a barrier between the apical and basolateral compartments. To test substrates, the unidirectional permeability (P_{app}) of a test compound was measured by dosing the compound separately to the apical side (for A > B P_{app}) and the basolateral side (for B > A P_{app}) of the cell monolayer. The movement of the compound into the respective receiver compartments was then monitored over a 3 h incubation period at 37 °C. The effect of P-gp was quantified by calculating the efflux ratio (ER) of the unidirectional apparent permeability coefficient (P_{app}). To determine the mean permeability in the absence of P-gp activity, the selective inhibitor zosuquidar was added at a concentration of 1 μM.

Determination of Plasma Protein Binding Values. Pooled and frozen plasma from human and mouse sources were procured from BioreclamationIVT.[77,78] The Teflon equilibrium dialysis plate (96-well, 150 μL half-cell capacity) and cellulose membranes with a molecular weight cutoff of 12−14 kDa were obtained from HT-Dialysis (Gales Ferry). On the day of the experiment, both the biological matrix and the phosphate buffer were adjusted to a pH of 7.4. The determination of unbound compounds was carried out using a 96-well format equilibrium dialysis device equipped with a 12−14 kDa molecular-weight cutoff membrane. The device, made of Teflon, was designed to minimize nonspecific binding of the test substances. Compounds were tested at an initial total concentration of 1000 nM, with diazepam included as a positive control. Equal volumes of matrix samples containing the test substances and blank dialysis buffer (Soerensen buffer at pH 7.4) were loaded into the opposite compartments of each well. The dialysis block was then sealed and incubated for 5 h at 37 °C in a 5% CO_2 environment. After this period, equilibrium was typically reached for most small-molecule compounds with a molecular weight of less than 600. The seal was then removed, and samples from both the matrix and buffer compartments were prepared for analysis using LC−MS/MS. All protein binding determinations were performed in triplicate. The integrity of the membranes was verified by determining the unbound fraction values for the positive control, diazepam, in each well. At equilibrium, the unbound drug concentration in the biological matrix compartment was equal to the concentration in the buffer compartment. The percentage of the unbound fraction (fu) was calculated using the following formula: % fu = 100 × (buffer concentration after dialysis/matrix concentration after dialysis). Device recovery was assessed by measuring the compound concentrations in the matrix before dialysis and calculating the percent recovery (mass balance), which needed to be within 80−120% for the data to be accepted.

Pharmacokinetic Studies in Male C57BL/6 Mice. The pharmacokinetics (PK) of the test compound was assessed in male C57BL/6 mice following intravenous (i.v.) administration at 3 mg/kg [as solution in *N*-methyl-2-pyrrolidone/NaCl-solution (0.9%) 30:70, 2 mL/kg], peroral (p.o.) administration at 5 mg/kg and intraperitoneal (i.p.) administration at 25 mg/kg (both as a suspension in *N*-methyl-2-pyrrolidone/hydroxypropyl methylcellulose/diisooctyl sulfosuccinate 10:90, 4 mL/kg). A total of 12 mice (N = 3 per i.v. and p.o. group, 6 in the i.p. group) received a single i.v., p.o., or i.p. dosing. Blood samples were collected at 0.083 (i.v. only), 0.25, 0.5, 1, 2, 4, and 7 h postdose. Brain and CSF samples were collected at 0.5, 2, and 7 h postdose in the i.p. group only with 2 animals sacrificed per time point (and consequently blood sampling times as described before with a decreasing number of animals over time). Blood samples were collected by using K2EDTA as the anticoagulant and placed on wet ice. Within half an hour of collection, the blood samples were processed for plasma by centrifugation at 3000*g* for 15 min at 4 °C. Following centrifugation, the plasma was separated and stored at −70 °C until analysis. Brain samples were homogenized with 3 volumes (w/v) of homogenization buffer (water). The compound concentrations in the plasma, CSF and brain were determined using LC−MS/MS. The pharmacokinetic parameters were obtained by noncompartmental analysis.

Pharmacokinetic Studies in Male Wistar Rats. The pharmacokinetics of the test compound was assessed in male Wistar rats following intravenous (i.v.) administration at 1 mg/kg (as solution in NMP/NaCl-solution (0.9%) 30:70, 2 mL/kg), peroral (p.o.) administration at 5 mg/kg, and intraperitoneal (i.p.) administration at 15 mg/kg (both as a solution in *N*-methyl-2-pyrrolidone/hydroxypropyl methylcellulose/diisooctyl sulfosuccinate 10:90, 4 mL/kg). A total of 12 rats (N = 3 per i.v. and p.o. group, 6 in the i.p. group) received a single i.v., p.o., or i.p. dosing. Blood samples were collected at 0.083 (i.v. only), 0.25, 0.5, 1, 2, 4, 7, and 24 (i.v. and p.o. only) hours postdose. Brain and CSF samples were collected at 1, 2, and 7 h postdose in the i.p. group only with 2 animals sacrificed per time point (and consequently blood sampling times as described before with a decreasing number of animals over time). Blood samples were collected using K2EDTA as the anticoagulant and placed on wet ice. Within half an hour of collection, the blood samples were processed for plasma by centrifugation at 3000*g* for 15 min at 4 °C. Following centrifugation, the plasma was separated and stored at −70 °C until analysis. Brain samples were homogenized with 3 volumes (w/v) of homogenization buffer (water). The compound concentrations in the plasma, CSF and brain were determined using LC−MS/MS. The pharmacokinetic parameters were obtained by noncompartmental analysis.

Chemistry. Chemistry procedures are detailed in the Supporting Information (S11−S105). All compounds are >95% pure by HPLC analysis.

■ ASSOCIATED CONTENT

Supporting Information

The Supporting Information is available free of charge at https://pubs.acs.org/doi/10.1021/acs.jmedchem.4c01769.

Focused screening hit rates; overlay of MAGL cocrystal structures with compounds **7a**, **2**, and **4**; X-ray cocrystal structure of human MAGL with compound **7i**; conformational analysis of compounds from crystal structures PDB: 9F8A, 9F8B, and 9F8C; selectivity profiling of **7o** against a diversity panel of 50 proteins; gel-based ABPP selectivity profiling of compound **7o**; X-ray data collection and refinement statistics; and chemistry procedures (PDF)

Molecular formula strings (CSV)

■ AUTHOR INFORMATION

Corresponding Authors

Bernd Kuhn − *Roche Pharma Research and Early Development, Roche Innovation Center Basel, F. Hoffmann-La Roche Ltd., Basel 4070, Switzerland*; orcid.org/0000-0002-4301-562X; Email: bernd.kuhn@roche.com

Uwe Grether − *Roche Pharma Research and Early Development, Roche Innovation Center Basel, F. Hoffmann-La Roche Ltd., Basel 4070, Switzerland*; orcid.org/0000-0002-3164-9270; Email: uwe.grether@roche.com

Authors

Martin Ritter − *Roche Pharma Research and Early Development, Roche Innovation Center Basel, F. Hoffmann-La Roche Ltd., Basel 4070, Switzerland*

Benoit Hornsperger − *Roche Pharma Research and Early Development, Roche Innovation Center Basel, F. Hoffmann-La Roche Ltd., Basel 4070, Switzerland*

Charles Bell − *Roche Pharma Research and Early Development, Roche Innovation Center Basel, F. Hoffmann-La Roche Ltd., Basel 4070, Switzerland*
Buelent Kocer − *Roche Pharma Research and Early Development, Roche Innovation Center Basel, F. Hoffmann-La Roche Ltd., Basel 4070, Switzerland*
Didier Rombach − *Roche Pharma Research and Early Development, Roche Innovation Center Basel, F. Hoffmann-La Roche Ltd., Basel 4070, Switzerland*
Marius D. R. Lutz − *Roche Pharma Research and Early Development, Roche Innovation Center Basel, F. Hoffmann-La Roche Ltd., Basel 4070, Switzerland;* orcid.org/0000-0003-3842-2295
Luca Gobbi − *Roche Pharma Research and Early Development, Roche Innovation Center Basel, F. Hoffmann-La Roche Ltd., Basel 4070, Switzerland;* orcid.org/0000-0002-0563-2491
Martin Kuratli − *Roche Pharma Research and Early Development, Roche Innovation Center Basel, F. Hoffmann-La Roche Ltd., Basel 4070, Switzerland*
Christian Bartelmus − *Roche Pharma Research and Early Development, Roche Innovation Center Basel, F. Hoffmann-La Roche Ltd., Basel 4070, Switzerland;* orcid.org/0000-0002-1527-4325
Markus Bürkler − *Roche Pharma Research and Early Development, Roche Innovation Center Basel, F. Hoffmann-La Roche Ltd., Basel 4070, Switzerland*
Raffael Koller − *Roche Pharma Research and Early Development, Roche Innovation Center Basel, F. Hoffmann-La Roche Ltd., Basel 4070, Switzerland*
Paolo Tosatti − *Roche Pharma Research and Early Development, Roche Innovation Center Basel, F. Hoffmann-La Roche Ltd., Basel 4070, Switzerland*
Iris Ruf − *Roche Pharma Research and Early Development, Roche Innovation Center Basel, F. Hoffmann-La Roche Ltd., Basel 4070, Switzerland*
Melanie Guerard − *Roche Pharma Research and Early Development, Roche Innovation Center Basel, F. Hoffmann-La Roche Ltd., Basel 4070, Switzerland*
Anto Pavlovic − *Roche Pharma Research and Early Development, Roche Innovation Center Basel, F. Hoffmann-La Roche Ltd., Basel 4070, Switzerland;* orcid.org/0009-0002-9395-6740
Juliane Stephanus − *Roche Pharma Research and Early Development, Roche Innovation Center Basel, F. Hoffmann-La Roche Ltd., Basel 4070, Switzerland*
Fionn O'Hara − *Roche Pharma Research and Early Development, Roche Innovation Center Basel, F. Hoffmann-La Roche Ltd., Basel 4070, Switzerland*
Dennis Wetzl − *Roche Pharma Research and Early Development, Roche Innovation Center Basel, F. Hoffmann-La Roche Ltd., Basel 4070, Switzerland*
Wiebke Saal − *Roche Pharma Research and Early Development, Roche Innovation Center Basel, F. Hoffmann-La Roche Ltd., Basel 4070, Switzerland*
Martine Stihle − *Roche Pharma Research and Early Development, Roche Innovation Center Basel, F. Hoffmann-La Roche Ltd., Basel 4070, Switzerland*
Doris Roth − *Roche Pharma Research and Early Development, Roche Innovation Center Basel, F. Hoffmann-La Roche Ltd., Basel 4070, Switzerland*
Melanie Hug − *Roche Pharma Research and Early Development, Roche Innovation Center Basel, F. Hoffmann-La Roche Ltd., Basel 4070, Switzerland*
Sylwia Huber − *Roche Pharma Research and Early Development, Roche Innovation Center Basel, F. Hoffmann-La Roche Ltd., Basel 4070, Switzerland*
Dominik Heer − *Roche Pharma Research and Early Development, Roche Innovation Center Basel, F. Hoffmann-La Roche Ltd., Basel 4070, Switzerland;* orcid.org/0009-0003-2089-4339
Carsten Kroll − *Roche Pharma Research and Early Development, Roche Innovation Center Basel, F. Hoffmann-La Roche Ltd., Basel 4070, Switzerland;* orcid.org/0009-0005-8255-326X
Andreas Topp − *Roche Pharma Research and Early Development, Roche Innovation Center Basel, F. Hoffmann-La Roche Ltd., Basel 4070, Switzerland*
Manfred Schneider − *Roche Pharma Research and Early Development, Roche Innovation Center Basel, F. Hoffmann-La Roche Ltd., Basel 4070, Switzerland*
Jürg Gertsch − *Institute of Biochemistry and Molecular Medicine, NCCR TransCure, University of Bern, Bern 3012, Switzerland;* orcid.org/0000-0003-0978-1555
Sandra Glasmacher − *Institute of Biochemistry and Molecular Medicine, NCCR TransCure, University of Bern, Bern 3012, Switzerland*
Mario van der Stelt − *Department of Molecular Physiology, Leiden Institute of Chemistry, Leiden University and Oncode Institute, Leiden 2300 CC, Netherlands;* orcid.org/0000-0002-1029-5717
Andrea Martella − *Department of Molecular Physiology, Leiden Institute of Chemistry, Leiden University and Oncode Institute, Leiden 2300 CC, Netherlands*
Matthias Beat Wittwer − *Roche Pharma Research and Early Development, Roche Innovation Center Basel, F. Hoffmann-La Roche Ltd., Basel 4070, Switzerland;* orcid.org/0000-0003-1359-4795
Ludovic Collin − *Roche Pharma Research and Early Development, Roche Innovation Center Basel, F. Hoffmann-La Roche Ltd., Basel 4070, Switzerland*
Jörg Benz − *Roche Pharma Research and Early Development, Roche Innovation Center Basel, F. Hoffmann-La Roche Ltd., Basel 4070, Switzerland*
Hans Richter − *Roche Pharma Research and Early Development, Roche Innovation Center Basel, F. Hoffmann-La Roche Ltd., Basel 4070, Switzerland*

Complete contact information is available at: https://pubs.acs.org/10.1021/acs.jmedchem.4c01769

Notes

The authors declare no competing financial interest.
Atomic coordinates of the X-ray crystal structures of human MAGL with compounds **7a**, **7n**, **7m**, and **7i** are deposited in the Protein Data Bank (PDB) under accession codes 9F8A, 9F8B, 9F8C, and 9F8D. The authors will release the atomic coordinates upon article publication.

■ ACKNOWLEDGMENTS

We thank Torsten Schindler for support in selecting the library for the focused screen. The synthetic contributions of Qiu Yangcheng and the WuXi team as well as from Pierre Schmitt

(Roche) are greatly acknowledged. Björn Wagner is thanked for the measurement of physicochemical properties.

■ ABBREVIATIONS

2-AG, 2-arachidonylglycerol; AA, arachidonic acid; ABHD12 and ABHD6, α,β-hydrolase domain containing protein 12 and 6; ABPP, activity-based protein profiling; ADME, absorption, distribution, metabolism, and excretion; AEA, *N*-arachidonoylethanolamine; AUC, area under the curve; B/P ratio, brain-to-plasma ratio; CB_1R, CB_2R, type-1 and type-2 cannabinoid receptors; CL, clearance; CNS, central nervous system; eCB, endocannabinoid; ECFP-6, extended connectivity fingerprints, diameter of bond distance 6; ECS, endocannabinoid system; *F*, bioavailability; FAAH, fatty acid amide hydrolase; hERG, human ether-à-go-go-related gene; HHPO, hexahydro-pyrido-oxazinone; IL1b, interleukin 1beta; i.p., intraperitoneal; i.v., intravenous; LCN2, lipocalin-2; LE, ligand efficiency; LIMBA, lipid membrane binding assay; LPS, lipopolysaccharide; LYSA, lyophilization solubility assay; MAGL, monoacylglycerol lipase; MNT, micronucleus test; MOS, maximum overlapping spheres; PAMPA, parallel artificial membrane permeability assay; P_{app}, apparent permeability; PET, positron emission tomography; PK, pharmacokinetics; PLA2, phospholipase A2; p.o., per os; QM, quantum-mechanical; qRT-PCR, quantitative reverse transcription polymerase chain reaction; SPR, surface plasmon resonance; $T_{1/2}$, half-life; V_{ss}, volume of distribution

■ REFERENCES

(1) Karlsson, M.; Contreras, J. A.; Hellman, U.; Tornqvist, H.; Holm, C. cDNA Cloning, Tissue Distribution, and Identification of the Catalytic Triad of Monoglyceride Lipase. *J. Biol. Chem.* **1997**, *272* (43), 27218−27223.

(2) Maccarrone, M.; Di Marzo, V.; Gertsch, J.; Grether, U.; Howlett, A. C.; Hua, T.; Makriyannis, A.; Piomelli, D.; Ueda, N.; van der Stelt, M. Goods and Bads of the Endocannabinoid System as a Therapeutic Target: Lessons Learned after 30 Years. *Pharmacol. Rev.* **2023**, *75* (5), 885−958.

(3) Hillard, C. J. Circulating Endocannabinoids: From Whence Do They Come and Where Are They Going? *Neuropsychopharmacology* **2018**, *43* (1), 155−172.

(4) Howlett, A. C.; Bidaut-Russell, M.; Devane, W. A.; Melvin, L. S.; Johnson, M. R.; Herkenham, M. The Cannabinoid Receptor: Biochemical, Anatomical and Behavioral Characterization. *Trends Neurosci.* **1990**, *13* (10), 420−423.

(5) Mackie, K.; Devane, W. A.; Hille, B. Anandamide, an Endogenous Cannabinoid, Inhibits Calcium Currents as a Partial Agonist in N18 Neuroblastoma Cells. *Mol. Pharmacol.* **1993**, *44* (3), 498−503.

(6) Felder, C. C.; Briley, E. M.; Axelrod, J.; Simpson, J. T.; Mackie, K.; Devane, W. A. Anandamide, an Endogenous Cannabimimetic Eicosanoid, Binds to the Cloned Human Cannabinoid Receptor and Stimulates Receptor-Mediated Signal Transduction. *Proc. Natl. Acad. Sci. U.S.A.* **1993**, *90* (16), 7656−7660.

(7) Shen, M.; Piser, T. M.; Seybold, V. S.; Thayer, S. A. Cannabinoid Receptor Agonists Inhibit Glutamatergic Synaptic Transmission in Rat Hippocampal Cultures. *J. Neurosci.* **1996**, *16* (14), 4322−4334.

(8) Glass, M.; Northup, J. K. Agonist Selective Regulation of G Proteins by Cannabinoid CB1 and CB2 Receptors. *Mol. Pharmacol.* **1999**, *56* (6), 1362−1369.

(9) Morisset, V.; Ahluwalia, J.; Nagy, I.; Urban, L. Possible Mechanisms of Cannabinoid-Induced Antinociception in the Spinal Cord. *Eur. J. Pharmacol.* **2001**, *429* (1−3), 93−100.

(10) Derkinderen, P.; Valjent, E.; Toutant, M.; Corvol, J.-C.; Enslen, H.; Ledent, C.; Trzaskos, J.; Caboche, J.; Girault, J.-A. Regulation of Extracellular Signal-Regulated Kinase by Cannabinoids in Hippocampus. *J. Neurosci.* **2003**, *23* (6), 2371−2382.

(11) Stella, N.; Schweitzer, P.; Piomelli, D. A Second Endogenous Cannabinoid That Modulates Long-Term Potentiation. *Nature* **1997**, *388* (6644), 773−778.

(12) Long, J. Z.; Nomura, D. K.; Cravatt, B. F. Characterization of Monoacylglycerol Lipase Inhibition Reveals Differences in Central and Peripheral Endocannabinoid Metabolism. *Chem. Biol.* **2009**, *16* (7), 744−753.

(13) Serhan, C. N.; Chiang, N.; Van Dyke, T. E. Resolving Inflammation: Dual Anti-Inflammatory and pro-Resolution Lipid Mediators. *Nat. Rev. Immunol.* **2008**, *8* (5), 349−361.

(14) Mulvihill, M. M.; Nomura, D. K. Therapeutic Potential of Monoacylglycerol Lipase Inhibitors. *Life Sci.* **2013**, *92* (8−9), 492−497.

(15) Bhattacharya, S.; Patel, R.; Sen, N.; Quadri, S.; Parthasarathi, K.; Bhattacharya, J. Dual signaling by the $\alpha_v\beta_3$-integrin activates cytosolic PLA_2in bovine pulmonary artery endothelial cells. *Am. J. Physiol. Lung Cell Mol. Physiol.* **2001**, *280* (5), L1049−L1056.

(16) Wang, B.; Wu, L.; Chen, J.; Dong, L.; Chen, C.; Wen, Z.; Hu, J.; Fleming, I.; Wang, D. W. Metabolism Pathways of Arachidonic Acids: Mechanisms and Potential Therapeutic Targets. *Signal Transduct. Targeted Ther.* **2021**, *6* (1), 94.

(17) Viader, A.; Blankman, J. L.; Zhong, P.; Liu, X.; Schlosburg, J. E.; Joslyn, C. M.; Liu, Q.-S.; Tomarchio, A. J.; Lichtman, A. H.; Selley, D. E.; Sim-Selley, L. J.; Cravatt, B. F. Metabolic Interplay between Astrocytes and Neurons Regulates Endocannabinoid Action. *Cell Rep.* **2015**, *12* (5), 798−808.

(18) Nomura, D. K.; Long, J. Z.; Niessen, S.; Hoover, H. S.; Ng, S.-W.; Cravatt, B. F. Monoacylglycerol Lipase Regulates a Fatty Acid Network That Promotes Cancer Pathogenesis. *Cell* **2010**, *140* (1), 49−61.

(19) Cao, Z.; Mulvihill, M. M.; Mukhopadhyay, P.; Xu, H.; Erdélyi, K.; Hao, E.; Holovac, E.; Haskó, G.; Cravatt, B. F.; Nomura, D. K.; Pacher, P. Monoacylglycerol Lipase Controls Endocannabinoid and Eicosanoid Signaling and Hepatic Injury in Mice. *Gastroenterology* **2013**, *144* (4), 808−817.

(20) Lomazzo, E.; Bindila, L.; Remmers, F.; Lerner, R.; Schwitter, C.; Hoheisel, U.; Lutz, B. Therapeutic Potential of Inhibitors of Endocannabinoid Degradation for the Treatment of Stress-Related Hyperalgesia in an Animal Model of Chronic Pain. *Neuropsychopharmacology* **2015**, *40* (2), 488−501.

(21) Jiang, M.; Huizenga, M. C. W.; Wirt, J. L.; Paloczi, J.; Amedi, A.; van den Berg, R. J. B. H. N.; Benz, J.; Collin, L.; Deng, H.; Di, X.; Driever, W. F.; Florea, B. I.; Grether, U.; Janssen, A. P. A.; Hankemeier, T.; Heitman, L. H.; Lam, T.-W.; Mohr, F.; Pavlovic, A.; Ruf, I.; van den Hurk, H.; Stevens, A. F.; van der Vliet, D.; van der Wel, T.; Wittwer, M. B.; van Boeckel, C. A. A.; Pacher, P.; Hohmann, A. G.; van der Stelt, M. A monoacylglycerol lipase inhibitor showing therapeutic efficacy in mice without central side effects or dependence. *Nat. Commun.* **2023**, *14* (1), 8039.

(22) Kinsey, S. G.; Long, J. Z.; O'Neal, S. T.; Abdullah, R. A.; Poklis, J. L.; Boger, D. L.; Cravatt, B. F.; Lichtman, A. H. Blockade of Endocannabinoid-Degrading Enzymes Attenuates Neuropathic Pain. *J. Pharmacol. Exp. Ther.* **2009**, *330* (3), 902−910.

(23) Brindisi, M.; Maramai, S.; Gemma, S.; Brogi, S.; Grillo, A.; Di Cesare Mannelli, L.; Gabellieri, E.; Lamponi, S.; Saponara, S.; Gorelli, B.; Tedesco, D.; Bonfiglio, T.; Landry, C.; Jung, K.-M.; Armirotti, A.; Luongo, L.; Ligresti, A.; Piscitelli, F.; Bertucci, C.; Dehouck, M.-P.; Campiani, G.; Maione, S.; Ghelardini, C.; Pittaluga, A.; Piomelli, D.; Di Marzo, V.; Butini, S. Development and Pharmacological Characterization of Selective Blockers of 2-Arachidonoyl Glycerol Degradation with Efficacy in Rodent Models of Multiple Sclerosis and Pain. *J. Med. Chem.* **2016**, *59* (6), 2612−2632.

(24) Kerr, D. M.; Harhen, B.; Okine, B. N.; Egan, L. J.; Finn, D. P.; Roche, M. The Monoacylglycerol Lipase Inhibitor JZL184 Attenuates LPS-Induced Increases in Cytokine Expression in the Rat Frontal Cortex and Plasma: Differential Mechanisms of Action. *Br. J. Pharmacol.* **2013**, *169* (4), 808−819.

https://doi.org/10.1021/acs.jmedchem.4c01769
J. Med. Chem. 2024, 67, 18448−18464

(25) Deng, H.; Li, W. Monoacylglycerol Lipase Inhibitors: Modulators for Lipid Metabolism in Cancer Malignancy, Neurological and Metabolic Disorders. *Acta Pharm. Sin. B* **2020**, *10* (4), 582−602.
(26) League, A. F.; Gorman, B. L.; Hermes, D. J.; Johnson, C. T.; Jacobs, I. R.; Yadav-Samudrala, B. J.; Poklis, J. L.; Niphakis, M. J.; Cravatt, B. F.; Lichtman, A. H.; et al. Monoacylglycerol Lipase Inhibitor MJN110 Reduces Neuronal Hyperexcitability, Restores Dendritic Arborization Complexity, and Regulates Reward-Related Behavior in Presence of HIV-1 Tat. *Front. Neurol.* **2021**, *12*, 651272.
(27) Zanfirescu, A.; Ungurianu, A.; Mihai, D. P.; Radulescu, D.; Nitulescu, G. M. Targeting Monoacylglycerol Lipase in Pursuit of Therapies for Neurological and Neurodegenerative Diseases. *Molecules* **2021**, *26* (18), 5668.
(28) Schlosburg, J. E.; Blankman, J. L.; Long, J. Z.; Nomura, D. K.; Pan, B.; Kinsey, S. G.; Nguyen, P. T.; Ramesh, D.; Booker, L.; Burston, J. J.; Thomas, E. A.; Selley, D. E.; Sim-Selley, L. J.; Liu, Q.; Lichtman, A. H.; Cravatt, B. F. Chronic Monoacylglycerol Lipase Blockade Causes Functional Antagonism of the Endocannabinoid System. *Nat. Neurosci.* **2010**, *13* (9), 1113−1119.
(29) Müller-Vahl, K. R.; Fremer, C.; Beals, C.; Ivkovic, J.; Loft, H.; Schindler, C. Monoacylglycerol Lipase Inhibition in Tourette Syndrome: A 12-Week, Randomized, Controlled Study. *Mov. Disord.* **2021**, *36* (10), 2413−2418.
(30) van Esbroeck, A. C. M.; Janssen, A. P. A.; Cognetta, A. B.; Ogasawara, D.; Shpak, G.; van der Kroeg, M.; Kantae, V.; Baggelaar, M. P.; de Vrij, F. M. S.; Deng, H.; Allarà, M.; Fezza, F.; Lin, Z.; van der Wel, T.; Soethoudt, M.; Mock, E. D.; den Dulk, H.; Baak, I. L.; Florea, B. I.; Hendriks, G.; De Petrocellis, L.; Overkleeft, H. S.; Hankemeier, T.; De Zeeuw, C. I.; Di Marzo, V.; Maccarrone, M.; Cravatt, B. F.; Kushner, S. A.; van der Stelt, M. Activity-Based Protein Profiling Reveals off-Target Proteins of the FAAH Inhibitor BIA 10−2474. *Science* **2017**, *356* (6342), 1084−1087.
(31) Granchi, C.; Caligiuri, I.; Minutolo, F.; Rizzolio, F.; Tuccinardi, T. A Patent Review of Monoacylglycerol Lipase (MAGL) Inhibitors (2013−2017). *Expert Opin. Ther. Pat.* **2017**, *27* (12), 1341−1351.
(32) Wiener, J. J. M.; Cisar, J. S.; Buzard, D. J.; Weber, O. D.; Grice, C. A. Development of Small-Molecule Inhibitors of Monoacylglycerol Lipase for the Treatment of Neurologic Diseases. In *2018 Medicinal Chemistry Reviews*; ACS, 2018; pp 463−478.
(33) Bononi, G.; Poli, G.; Rizzolio, F.; Tuccinardi, T.; Macchia, M.; Minutolo, F.; Granchi, C. An Updated Patent Review of Monoacylglycerol Lipase (MAGL) Inhibitors (2018-Present). *Expert Opin. Ther. Pat.* **2021**, *31* (2), 153−168.
(34) Bertrand, T.; Augé, F.; Houtmann, J.; Rak, A.; Vallée, F.; Mikol, V.; Berne, P. F.; Michot, N.; Cheuret, D.; Hoornaert, C.; Mathieu, M. Structural Basis for Human Monoglyceride Lipase Inhibition. *J. Mol. Biol.* **2010**, *396* (3), 663−673.
(35) Cisar, J. S.; Weber, O. D.; Clapper, J. R.; Blankman, J. L.; Henry, C. L.; Simon, G. M.; Alexander, J. P.; Jones, T. K.; Ezekowitz, R. A. B.; O'Neill, G. P.; Grice, C. A. Identification of ABX-1431, a Selective Inhibitor of Monoacylglycerol Lipase and Clinical Candidate for Treatment of Neurological Disorders. *J. Med. Chem.* **2018**, *61* (20), 9062−9084.
(36) McAllister, L. A.; Butler, C. R.; Mente, S.; O'Neil, S. V.; Fonseca, K. R.; Piro, J. R.; Cianfrogna, J. A.; Foley, T. L.; Gilbert, A. M.; Harris, A. R.; Helal, C. J.; Johnson, D. S.; Montgomery, J. I.; Nason, D. M.; Noell, S.; Pandit, J.; Rogers, B. N.; Samad, T. A.; Shaffer, C. L.; da Silva, R. G.; Uccello, D. P.; Webb, D.; Brodney, M. A. Discovery of Trifluoromethyl Glycol Carbamates as Potent and Selective Covalent Monoacylglycerol Lipase (MAGL) Inhibitors for Treatment of Neuroinflammation. *J. Med. Chem.* **2018**, *61* (7), 3008−3026.
(37) Butini, S.; Grether, U.; Jung, K.-M.; Ligresti, A.; Allarà, M.; Postmus, A. G. J.; Maramai, S.; Brogi, S.; Papa, A.; Carullo, G.; Sykes, D.; Veprintsev, D.; Federico, S.; Grillo, A.; Di Guglielmo, B.; Ramunno, A.; Stevens, A. F.; Heer, D.; Lamponi, S.; Gemma, S.; Benz, J.; Di Marzo, V.; van der Stelt, M.; Piomelli, D.; Campiani, G. Development of Potent and Selective Monoacylglycerol Lipase Inhibitors. SARs, Structural Analysis, and Biological Characterization. *J. Med. Chem.* **2024**, *67* (3), 1758−1782.
(38) Jiang, M.; Huizenga, M. C. W.; Mohr, F.; Amedi, A.; Bakker, R.; van den Berg, R. J. B. H. N.; Deng, H.; van der Wel, T.; van Boeckel, C. A. A.; van der Stelt, M. Structure-Activity Relationship Studies of Aryl Sulfoxides as Reversible Monoacylglycerol Lipase Inhibitors. *J. Med. Chem.* **2024**, *67* (14), 12331−12348.
(39) Granchi, C.; Rizzolio, F.; Palazzolo, S.; Carmignani, S.; Macchia, M.; Saccomanni, G.; Manera, C.; Martinelli, A.; Minutolo, F.; Tuccinardi, T. Structural Optimization of 4-Chlorobenzoylpiperidine Derivatives for the Development of Potent, Reversible, and Selective Monoacylglycerol Lipase (MAGL) Inhibitors. *J. Med. Chem.* **2016**, *59* (22), 10299−10314.
(40) Granchi, C.; Caligiuri, I.; Bertelli, E.; Poli, G.; Rizzolio, F.; Macchia, M.; Martinelli, A.; Minutolo, F.; Tuccinardi, T. Development of Terphenyl-2-Methyloxazol-5(4H)-One Derivatives as Selective Reversible MAGL Inhibitors. *J. Enzyme Inhib. Med. Chem.* **2017**, *32* (1), 1240−1252.
(41) Bononi, G.; Granchi, C.; Lapillo, M.; Giannotti, M.; Nieri, D.; Fortunato, S.; Boustani, M. E.; Caligiuri, I.; Poli, G.; Carlson, K. E.; Kim, S. H.; Macchia, M.; Martinelli, A.; Rizzolio, F.; Chicca, A.; Katzenellenbogen, J. A.; Minutolo, F.; Tuccinardi, T. Discovery of Long-Chain Salicylketoxime Derivatives as Monoacylglycerol Lipase (MAGL) Inhibitors. *Eur. J. Med. Chem.* **2018**, *157*, 817−836.
(42) Lauria, S.; Perrotta, C.; Casati, S.; Di Renzo, I.; Ottria, R.; Eberini, I.; Palazzolo, L.; Parravicini, C.; Ciuffreda, P. Design, Synthesis, Molecular Modelling and in Vitro Cytotoxicity Analysis of Novel Carbamate Derivatives as Inhibitors of Monoacylglycerol Lipase. *Bioorg. Med. Chem.* **2018**, *26* (9), 2561−2572.
(43) Aghazadeh Tabrizi, M.; Baraldi, P. G.; Baraldi, S.; Ruggiero, E.; De Stefano, L.; Rizzolio, F.; Di Cesare Mannelli, L.; Ghelardini, C.; Chicca, A.; Lapillo, M.; Gertsch, J.; Manera, C.; Macchia, M.; Martinelli, A.; Granchi, C.; Minutolo, F.; Tuccinardi, T. Discovery of 1,5-Diphenylpyrazole-3-Carboxamide Derivatives as Potent, Reversible, and Selective Monoacylglycerol Lipase (MAGL) Inhibitors. *J. Med. Chem.* **2018**, *61* (3), 1340−1354.
(44) Poli, G.; Lapillo, M.; Jha, V.; Mouawad, N.; Caligiuri, I.; Macchia, M.; Minutolo, F.; Rizzolio, F.; Tuccinardi, T.; Granchi, C. Computationally Driven Discovery of Phenyl(Piperazin-1-Yl)-Methanone Derivatives as Reversible Monoacylglycerol Lipase (MAGL) Inhibitors. *J. Enzyme Inhib. Med. Chem.* **2019**, *34* (1), 589−596.
(45) Granchi, C.; Lapillo, M.; Glasmacher, S.; Bononi, G.; Licari, C.; Poli, G.; el Boustani, M.; Caligiuri, I.; Rizzolio, F.; Gertsch, J.; Macchia, M.; Minutolo, F.; Tuccinardi, T.; Chicca, A. Optimization of a Benzoylpiperidine Class Identifies a Highly Potent and Selective Reversible Monoacylglycerol Lipase (MAGL) Inhibitor. *J. Med. Chem.* **2019**, *62* (4), 1932−1958.
(46) Dato, F. M.; Neudörfl, J.-M.; Gütschow, M.; Goldfuss, B.; Pietsch, M. ω-Quinazolinonylalkyl Aryl Ureas as Reversible Inhibitors of Monoacylglycerol Lipase. *Bioorg. Chem.* **2020**, *94*, 103352.
(47) Bononi, G.; Di Stefano, M.; Poli, G.; Ortore, G.; Meier, P.; Masetto, F.; Caligiuri, I.; Rizzolio, F.; Macchia, M.; Chicca, A.; Avan, A.; Giovannetti, E.; Vagaggini, C.; Brai, A.; Dreassi, E.; Valoti, M.; Minutolo, F.; Granchi, C.; Gertsch, J.; Tuccinardi, T. Reversible Monoacylglycerol Lipase Inhibitors: Discovery of a New Class of Benzylpiperidine Derivatives. *J. Med. Chem.* **2022**, *65* (10), 7118−7140.
(48) Di Stefano, M.; Masoni, S.; Bononi, G.; Poli, G.; Galati, S.; Gado, F.; Manzi, S.; Vagaggini, C.; Brai, A.; Caligiuri, I.; Asif, K.; Rizzolio, F.; Macchia, M.; Chicca, A.; Sodi, A.; Di Bussolo, V.; Minutolo, F.; Meier, P.; Gertsch, J.; Granchi, C.; Dreassi, E.; Tuccinardi, T. Design, Synthesis, ADME and Biological Evaluation of Benzylpiperidine and Benzylpiperazine Derivatives as Novel Reversible Monoacylglycerol Lipase (MAGL) Inhibitors. *Eur. J. Med. Chem.* **2024**, *263*, 115916.
(49) Schalk-Hihi, C.; Schubert, C.; Alexander, R.; Bayoumy, S.; Clemente, J. C.; Deckman, I.; DesJarlais, R. L.; Dzordzorme, K. C.; Flores, C. M.; Grasberger, B.; Kranz, J. K.; Lewandowski, F.; Liu, L.;

https://doi.org/10.1021/acs.jmedchem.4c01769
J. Med. Chem. 2024, 67, 18448−18464

Ma, H.; Maguire, D.; Macielag, M. J.; McDonnell, M. E.; Mezzasalma Haarlander, T.; Miller, R.; Milligan, C.; Reynolds, C.; Kuo, L. C. Crystal Structure of a Soluble Form of Human Monoglyceride Lipase in Complex with an Inhibitor at 1.35 Å Resolution. *Protein Sci.* **2011**, *20* (4), 670−683.
(50) Aida, J.; Fushimi, M.; Kusumoto, T.; Sugiyama, H.; Arimura, N.; Ikeda, S.; Sasaki, M.; Sogabe, S.; Aoyama, K.; Koike, T. Design, Synthesis, and Evaluation of Piperazinyl Pyrrolidin-2-Ones as a Novel Series of Reversible Monoacylglycerol Lipase Inhibitors. *J. Med. Chem.* **2018**, *61* (20), 9205−9217.
(51) Ikeda, S.; Sugiyama, H.; Tokuhara, H.; Murakami, M.; Nakamura, M.; Oguro, Y.; Aida, J.; Morishita, N.; Sogabe, S.; Dougan, D. R.; Gay, S. C.; Qin, L.; Arimura, N.; Takahashi, Y.; Sasaki, M.; Kamada, Y.; Aoyama, K.; Kimoto, K.; Kamata, M. Design and Synthesis of Novel Spiro Derivatives as Potent and Reversible Monoacylglycerol Lipase (MAGL) Inhibitors: Bioisosteric Transformation from 3-Oxo-3,4-Dihydro-2H-Benzo[b] [1,4]Oxazin-6-Yl Moiety. *J. Med. Chem.* **2021**, *64* (15), 11014−11044.
(52) Kemble, A. M.; Hornsperger, B.; Ruf, I.; Richter, H.; Benz, J.; Kuhn, B.; Heer, D.; Wittwer, M.; Engelhardt, B.; Grether, U.; Collin, L. A Potent and Selective Inhibitor for the Modulation of MAGL Activity in the Neurovasculature. *PLoS One* **2022**, *17* (9), No. e0268590.
(53) He, Y.; Schild, M.; Grether, U.; Benz, J.; Leibrock, L.; Heer, D.; Topp, A.; Collin, L.; Kuhn, B.; Wittwer, M.; Keller, C.; Gobbi, L. C.; Schibli, R.; Mu, L. Development of High Brain-Penetrant and Reversible Monoacylglycerol Lipase PET Tracers for Neuroimaging. *J. Med. Chem.* **2022**, *65* (3), 2191−2207.
(54) Haider, A.; Gobbi, L.; Kretz, J.; Ullmer, C.; Brink, A.; Honer, M.; Woltering, T. J.; Muri, D.; Iding, H.; Bürkler, M.; Binder, M.; Bartelmus, C.; Knuesel, I.; Pacher, P.; Herde, A. M.; Spinelli, F.; Ahmed, H.; Atz, K.; Keller, C.; Weber, M.; Schibli, R.; Mu, L.; Grether, U.; Ametamey, S. M. Identification and Preclinical Development of a 2,5,6-Trisubstituted Fluorinated Pyridine Derivative as a Radioligand for the Positron Emission Tomography Imaging of Cannabinoid Type 2 Receptors. *J. Med. Chem.* **2020**, *63* (18), 10287−10306.
(55) Bendels, S.; Bissantz, C.; Fasching, B.; Gerebtzoff, G.; Guba, W.; Kansy, M.; Migeon, J.; Mohr, S.; Peters, J.-U.; Tillier, F.; Wyler, R.; Lerner, C.; Kramer, C.; Richter, H.; Roberts, S. Safety Screening in Early Drug Discovery: An Optimized Assay Panel. *J. Pharmacol. Toxicol. Methods* **2019**, *99*, 106609.
(56) Janssen, A. P. A.; van der Vliet, D.; Bakker, A. T.; Jiang, M.; Grimm, S. H.; Campiani, G.; Butini, S.; van der Stelt, M. Development of a Multiplexed Activity-Based Protein Profiling Assay to Evaluate Activity of Endocannabinoid Hydrolase Inhibitors. *ACS Chem. Biol.* **2018**, *13* (9), 2406−2413.
(57) He, Y.; Grether, U.; Taddio, M. F.; Meier, C.; Keller, C.; Edelmann, M. R.; Honer, M.; Huber, S.; Wittwer, M. B.; Heer, D.; Richter, H.; Collin, L.; Hug, M. N.; Hilbert, M.; Postmus, A. G. J.; Stevens, A. F.; van der Stelt, M.; Krämer, S. D.; Schibli, R.; Mu, L.; Gobbi, L. C. Multi-Parameter Optimization: Development of a Morpholin-3-One Derivative with an Improved Kinetic Profile for Imaging Monoacylglycerol Lipase in the Brain. *Eur. J. Med. Chem.* **2022**, *243*, 114750.
(58) Sanguinetti, M. C.; Tristani-Firouzi, M. hERG Potassium Channels and Cardiac Arrhythmia. *Nature* **2006**, *440* (7083), 463−469.
(59) Fowler, S.; Zhang, H. In Vitro Evaluation of Reversible and Irreversible Cytochrome P450 Inhibition: Current Status on Methodologies and Their Utility for Predicting Drug-Drug Interactions. *AAPS J.* **2008**, *10* (2), 410−424.
(60) Brink, A.; Fontaine, F.; Marschmann, M.; Steinhuber, B.; Cece, E. N.; Zamora, I.; Pähler, A. Post-Acquisition Analysis of Untargeted Accurate Mass Quadrupole Time-of-Flight MS(E) Data for Multiple Collision-Induced Neutral Losses and Fragment Ions of Glutathione Conjugates. *Rapid Commun. Mass Spectrom.* **2014**, *28* (24), 2695−2703.
(61) Cumming, J. G.; Kreis, L.; Kühne, H.; Wermuth, R.; Vercruysse, M.; Cantrill, C.; Bissantz, C.; Qiu, H.; Kramer, C.; Andreotti, D.; Fossati, G. Novel Indane-Containing NBTIs with Potent Anti-Gram-Negative Activity and Minimal hERG Inhibition. *ACS Med. Chem. Lett.* **2023**, *14* (12), 1791−1799.
(62) Kang, S. S.; Ren, Y.; Liu, C.-C.; Kurti, A.; Baker, K. E.; Bu, G.; Asmann, Y.; Fryer, J. D. Lipocalin-2 Protects the Brain during Inflammatory Conditions. *Mol. Psychiatr.* **2018**, *23* (2), 344−350.
(63) Piro, J. R.; Suidan, G. L.; Quan, J.; Pi, Y.; O'Neill, S. M.; Ilardi, M.; Pozdnyakov, N.; Lanz, T. A.; Xi, H.; Bell, R. D.; Samad, T. A. Inhibition of 2-AG Hydrolysis Differentially Regulates Blood Brain Barrier Permeability after Injury. *J. Neuroinflammation* **2018**, *15*, 142.
(64) Hao, Q.; Shi, J.; Zhang, Z.; Yang, G.; Zhi, Y.; Wang, K.; Ma, D.; Fu, S.; Dong, H.; Zhi, Z.; Zhang, W.; Li, T.; Wang, J. Discovery of a Novel Class of Reversible Monoacylglycerol Lipase Inhibitors for Potential Treatment of Depression. *Eur. J. Med. Chem.* **2024**, *268*, 116285.
(65) He, Y.; Gobbi, L. C.; Herde, A. M.; Rombach, D.; Ritter, M.; Kuhn, B.; Wittwer, M. B.; Heer, D.; Hornsperger, B.; Bell, C.; O'Hara, F.; Benz, J.; Honer, M.; Keller, C.; Collin, L.; Richter, H.; Schibli, R.; Grether, U.; Mu, L. Discovery, Synthesis and Evaluation of Novel Reversible Monoacylglycerol Lipase Radioligands Bearing a Morpholine-3-One Scaffold. *Nucl. Med. Biol.* **2022**, *108*−*109*, 24−32.
(66) Rogers, D.; Hahn, M. Extended-Connectivity Fingerprints. *J. Chem. Inf. Model.* **2010**, *50* (5), 742−754.
(67) Stahl, M.; Mauser, H.; Tsui, M.; Taylor, N. R. A Robust Clustering Method for Chemical Structures. *J. Med. Chem.* **2005**, *48* (13), 4358−4366.
(68) Hawkins, P. C. D.; Skillman, A. G.; Nicholls, A. Comparison of Shape-Matching and Docking as Virtual Screening Tools. *J. Med. Chem.* **2007**, *50* (1), 74−82.
(69) Kabsch, W. XDS. *Acta Crystallogr., Sect. D: Biol. Crystallogr.* **2010**, *66* (2), 125−132.
(70) McCoy, A. J.; Grosse-Kunstleve, R. W.; Adams, P. D.; Winn, M. D.; Storoni, L. C.; Read, R. J. Phaser Crystallographic Software. *J. Appl. Crystallogr.* **2007**, *40* (4), 658−674.
(71) Winn, M. D.; Ballard, C. C.; Cowtan, K. D.; Dodson, E. J.; Emsley, P.; Evans, P. R.; Keegan, R. M.; Krissinel, E. B.; Leslie, A. G. W.; McCoy, A.; McNicholas, S. J.; Murshudov, G. N.; Pannu, N. S.; Potterton, E. A.; Powell, H. R.; Read, R. J.; Vagin, A.; Wilson, K. S. Overview of the CCP4 Suite and Current Developments. *Acta Crystallogr., Sect. D: Biol. Crystallogr.* **2011**, *67* (4), 235−242.
(72) Bricogne, G.; Blanc, G. E.; Brandl, M.; Flensburg, C.; Keller, P.; Paciorek, W.; Roversi, P.; Sharff, A.; Smart, O. S.; Vonrhein, C.; Womack, T. O. *Buster*, Version 2.9.5 Cambridge; Global Phasing Ltd.: United Kingdom, 2011.
(73) Emsley, P.; Lohkamp, B.; Scott, W. G.; Cowtan, K. Features and Development of Coot. *Acta Crystallogr., Sect. D: Biol. Crystallogr.* **2010**, *66* (4), 486−501.
(74) Wagner, B.; Fischer, H.; Kansy, M.; Seelig, A.; Assmus, F. Carrier Mediated Distribution System (CAMDIS): A New Approach for the Measurement of Octanol/Water Distribution Coefficients. *Eur. J. Pharm. Sci.* **2015**, *68*, 68−77.
(75) Chen, X.; Murawski, A.; Patel, K.; Crespi, C. L.; Balimane, P. V. A Novel Design of Artificial Membrane for Improving the PAMPA Model. *Pharm. Res.* **2008**, *25* (7), 1511−1520.
(76) Poirier, A.; Cascais, A.-C.; Bader, U.; Portmann, R.; Brun, M.-E.; Walter, I.; Hillebrecht, A.; Ullah, M.; Funk, C. Calibration of In Vitro Multidrug Resistance Protein 1 Substrate and Inhibition Assays as a Basis to Support the Prediction of Clinically Relevant Interactions In Vivo. *Drug Metab. Dispos.* **2014**, *42* (9), 1411−1422.
(77) Banker, M. J.; Clark, T. H.; Williams, J. A. Development and Validation of a 96-Well Equilibrium Dialysis Apparatus for Measuring Plasma Protein Binding. *J. Pharm. Sci.* **2003**, *92* (5), 967−974.
(78) Zamek-Gliszczynski, M. J.; Ruterbories, K. J.; Ajamie, R. T.; Wickremsinhe, E. R.; Pothuri, L.; Rao, M. V. S.; Basavanakatti, V. N.; Pinjari, J.; Ramanathan, V. K.; Chaudhary, A. K. Validation of 96-Well Equilibrium Dialysis with Non-Radiolabeled Drug for Definitive Measurement of Protein Binding and Application to Clinical

https://doi.org/10.1021/acs.jmedchem.4c01769
J. Med. Chem. 2024, 67, 18448−18464

Development of Highly-Bound Drugs. *J. Pharm. Sci.* **2011**, *100* (6), 2498−2507.

https://doi.org/10.1021/acs.jmedchem.4c01769
J. Med. Chem. 2024, 67, 18448−18464